CrossMark

Geothermal Energy Reconnaissance of Southeastern Nigeria from Analysis of Aeromagnetic and Gravity Data

EMA ABRAHAM,[1] ONYEKACHI ITUMOH,[1] CHIBUZO CHUKWU,[1] and ONWE ROCK[1]

Abstract—Given the daunting energy challenges currently bedeviling Nigeria, with demand for electrical power exceeding availability, alternative energy sources (preferentially renewable) are vigorously considered. This is the first study to examine geothermal energy prospects in southeastern Nigeria with the ultimate aim of locating and mapping regions of shallow Curie point depths (CPDs), crustal thickness, and geologic structures supportive of a geothermal system. We estimated CPD using the spectral analysis technique on magnetic field anomalies. Gravity anomalies were subjected to a series of procedures to assess geological structures. Result reveals deeper CPDs within central and southern regions of Okposi, Afikpo and Biase towns in an approximate range of 18.4 to 19.3 km. Shallow CPDs (9.8–17.4 km) have also been obtained within Obubra and Abakaliki regions. Estimated crustal thickness (Moho) ranges between 26.5 and 35.8 km. Part of the region with shallow CPD correlates with regions of shallow Moho depths, particularly in Abakaliki, and deeper Moho depths coincide with deeper CPD estimates at the Afikpo location. The estimated geothermal gradient and heat flow values range between 29.0 and 45.0 °C and 52.2–101.5 mW/m^2, respectively, and fall within values evaluated from deep wells drilled for oil exploration within the adjoining Anambra Basin region. This study recommends the regions with shallow depths for possible geothermal power plant location. Gravity data evaluations also reveal significant subsurface intrusions within Ugbodo, Obubra and Abakaliki locations. Overall, this study is a step forward toward a better evaluation of the geothermal energy resources potential of southeastern Nigeria.

Key words: Geothermal, aeromagnetic, gravity, Curie depths, heat flow, geologic structures.

1. Introduction

Exploitation of geothermal resources in Nigeria is essential given the country's daunting energy challenges and its status as a developing nation.

Geothermal resources abound in Nigeria and some surface manifestations in the form of warm springs have been previously located (Abraham and Nkitnam 2017). High geothermal gradients at some locations have also been documented (Nwachukwu 1976; Avbovbo 1978; Babalola 1984). The geology of Nigeria is classified into sedimentary basins and basement complex rocks (Fig. 1). The sedimentary basins include the Benue Trough, a synclinal structure trending NE–SW, and the oil-rich Niger Delta Basin as well as the Nupe or Bida, Sokoto and Chad or Borno Basins. The sediments of these Basins are mainly Cretaceous to recent and comprise a Y-shape structure extending from the northwestern and northeastern part of the country forming a delta as it offloads to the Atlantic Ocean. The coverage area of our study lies between geographic latitudes 5°00N′ and 7°00N′ and geographic longitudes 7°00E′ and 9°00E′. The area spans approximately 49,300 km^2 cutting across 9 political states in the region. Our study area also includes the entirety of the Abakaliki Anticlinorium, parts of the Anambra Basin to the west and the crystalline basement complex to the east and southeastern regions of Nigeria.

Although there are no surface manifestations in the form of hot springs in the region of focus, nevertheless, preliminary study conducted by Babalola (1984) concluded that geothermal gradients obtained in the region indicate that steam could be encountered at about 1.3 km in the Abakaliki region. He recommended a combination of heat flow measurements and analysis of existing aeromagnetic data to provide a basis for the determination of geothermal gradients in the undrilled resource areas including determination of depths to the Curie isotherm. Nwachukwu and Avbovbo studied the distribution of subsurface

[1] Department of Physics/Geology/Geophysics, Federal University Ndufu Alike Ikwo, Abakaliki 1010, Ebonyi, Nigeria. E-mail: ema.abraham@funai.edu.ng
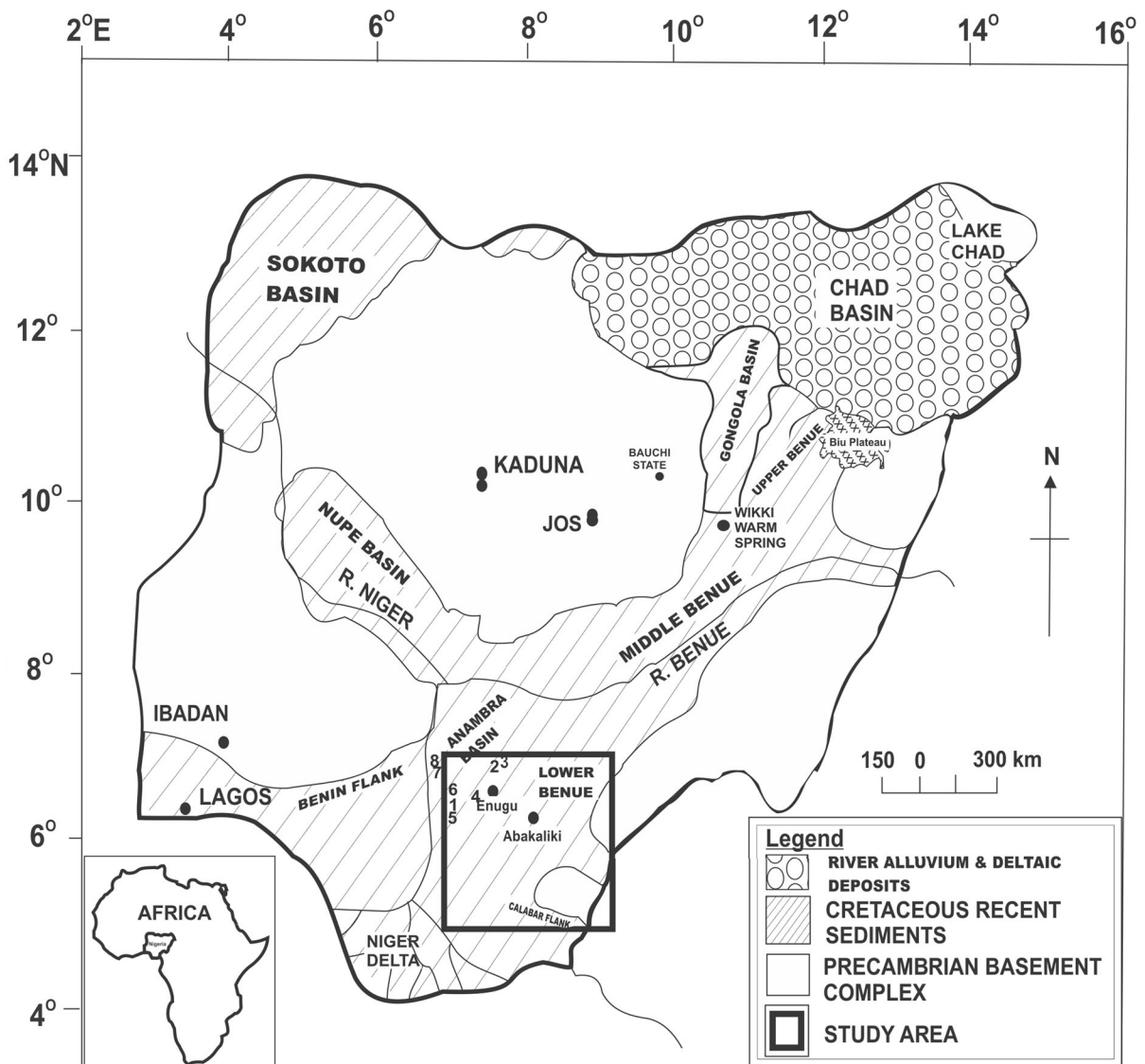
Figure 1
Map of Nigeria showing the general geology, location and coverage area of our study (modified from Abraham et al. 2014). The numbers around the study area represents some of the deep wells drilled for oil exploration (Onuoha and Ekine 1999): 1) well 1 GB-1 (thermal gradient = 46.30 °C/km); 2) well 1H-1 (57.30 °C/km); 3) well A1D (54.4 °C/km); 4) well AM-1 (42.35 °C/km); 5) well AK-2 (50.2 °C/km); 6) well LO-1 (52.77 °C/km); 7) well ANR-3 (28.45 °C/km); 8) well ANR-1 (35.44 °C/km)

temperature focusing on the southern part of the sedimentary province in Nigeria (Nwachukwu 1975, 1976; Avbovbo 1978). They used bottom hole temperature (BHT) data measured in oil exploration wells drilled in Niger Delta Basin and a small section of the Anambra Basin. From their analysis, the lowest values of geothermal gradient were found in the centre of the Niger Delta within the thick Tertiary sediments:

1.3–1.8 °C/100 m (Nwachukwu 1975) or 2.2–2.6 °C/100 m within the Warri-Port Harcourt region of the Niger Delta Basin (Avbovbo 1978). Kurowska and Schoeneich (2010) determined a northward trend of gradient increase resulting in a maximum value of 5.5 °C/100 m within the Cretaceous rocks of the basin. Ofoegbu and Onuoha (1991) attempted to determine the mean depths to the buried magnetic

basement around the Abakaliki anticlinorium using aeromagnetic data. Their results indicated depths to the deeper magnetic sources between 1200 and 2500 m. They concluded from their results that their study area in the Benue Trough may not hold much promise in terms of hydrocarbon accumulation. To assess the viability of petroleum exploration in some regions of the southern Benue Trough, Oha et al. (2016) interpreted aeromagnetic anomalies of the region. Results from their analysis indicated shallow magmatic bodies (< 200 m) within 40% of the sedimentary basin, mostly intermediate to mafic hyperbysal and intrusive rocks. Other studies connected to the analysis of aeromagnetic data in parts of the Benue Trough (Ajakaiye 1981; Ofoegbu 1985, 1984; Osazuwa et al. 1981; Nur 2000; Obi et al. 2010) abound, however, majority of these studies concentrated on assessing the petroleum resources prospects of the region. Little or no attention was given to the geothermal energy prospects of the region including the Abakaliki Basin (our study area) and environ. Nonetheless, a few studies (Nur et al. 1999; Onuoha and Ekine 1999; Obande et al. 2014; Abraham et al. 2015) endeavored to provide insights on the geothermal potentials of some parts of the Benue Trough. Onuoha and Ekine (1999) conducted the closest geothermal consideration of the lower Benue Trough. Their study covered an extensive portion of the Anambra Basin and was an attempt to assess the implication of subsurface temperatures and heat flow primarily for petroleum prospecting within Anambra Basin. They examined data from 16 deep wells drilled for oil exploration purposes in the basin and their results show geothermal gradients varying between 25 and 49 ± 1 °C, and heat flow ranging between 48–76 $\pm$ 3 mW/m^2. Onuoha and Ekine's study has been mentioned by Emujakporue and Nwosu as the only known geothermal research with substantive coverage of the Anambra sedimentary basin (Emujakporue and Nwosu 2017). This study is the first to examine the geothermal energy resource prospects in the region including part of the Anambra Basin and aims to investigate the basal depth of magnetic anomaly sources herewith referred as the Curie point depth (CPD) using recently acquired high-resolution aeromagnetic anomaly data. Average geothermal gradients and heat flow information are estimated

from the results. High-resolution satellite gravity data (Sandwell and Smith 2009) is also used to assess the structural control and crustal thickness supportive of geothermal resources in the study region.

2. Tectonic and Geologic Setting

The geological structure of an area influences the general distribution of geothermal heat in the upper earth crust and additionally, specifically for Nigeria, impacts geothermal exploration extent (Kurowska and Schoeneich 2010). The Basement Complex rocks consist of Precambrian to Lower Palaeozoic metamorphic and igneous rocks with tertiary to recent volcanic rocks. The Schist belts (metasediments and metavolcanics) which overlay the basement are dominant in the southern and western part of the Country (Ajibade and Fitches 1988). Cretaceous sediments connected with some volcanic satiates the Benue Trough up to 6000 m and forms part of a mega-rift system generally referred to as the West and Central Africa Rift System (WCARS; Obaje 2009; Abubakar 2014). Compressional folding that took place in the mid-Santonian tectonic episode influenced the entire Benue Trough and was quite intense, resulting in over 100 synclines and anticlines (Benkhelil 1989). Notable deformational structures in the lower Benue Trough include the Afikpo syncline and the Abakaliki anticlinorium (Obaje 2009). The Benue Trough, with regard to geography, is subdivided into lower (southern), Middle (central) and Upper (northern) regions (Fig. 1). Sedimentary Basin in southern Nigeria comprises the lower Benue Trough, Niger Delta Benin Embayment, the Anambra Basin, the Abakaliki fold belt (Abakaliki Anticlinorium), the Afikpo syncline and the Calabar flank (Fig. 1). Deposits within our study area range in age from Cretaceous to recent (Fig. 2). Various fault trends are notable in the region with dominant trends in the NE–SW directions. Upper Cretaceous to Tertiary volcanics occurs in the lower Benue Trough and the adjacent Cameroun volcanic ranges (Burke et al. 1972). Murat (1972) suggested that a late Eocene tectonism in the lower Benue Trough caused the NE–SW and NE–SE trending faults in the region. Within this sedimentary basin, sedimentation was controlled
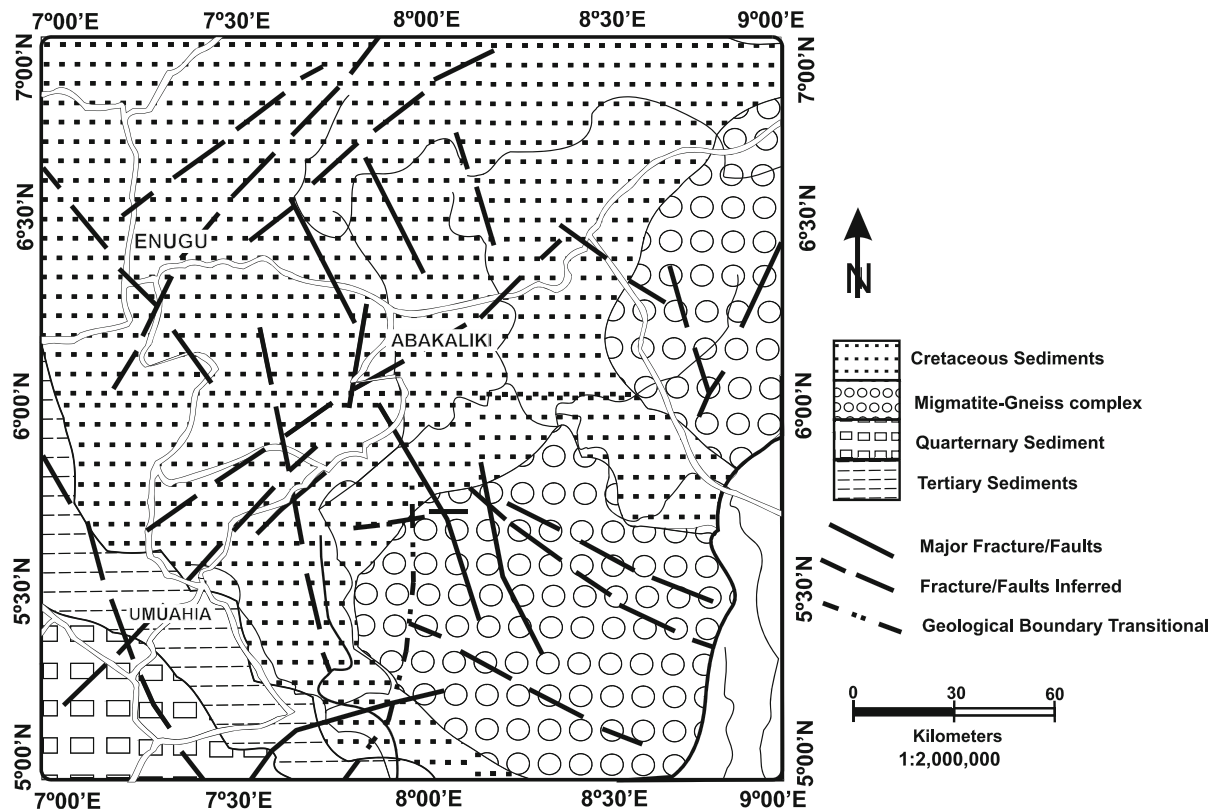
Figure 2
Tectonic setting of the study area [extracted from lineament map of Nigeria: courtesy of the Nigerian Geological Survey Agency (NGSA)]. A majority of the fault structures trend in the NE–SW directions. The Cretaceous sedimentation houses a majority of the fault structures with some criss-crosses. This region is part of the Benue Trough on which sedimentation started in the Aptian, and culminated in the development of the Tertiary Niger Delta. The sequence started with lava flows and volcanioclastics of the Abakaliki pyroclastics which predate the Albian transgression that initiated marine deposition in the trough (Agagu and Adighije 1983)

by a number of tectonic elements, namely the Benue and Abakaliki Troughs, the Calabar and Benin flanks and the uplift at the Abakaliki axis (Nwachukwu 1975). Some tectonic phases, together with the accompanying transgressive and regressive cycles, have been recognized (Short and Stauble 1967; Murat 1972; Nwachukwu 1975; Obi et al. 2001; Oboh-Ikuenobe et al. 2005), such as the Abakaliki–Benue phase (Aptian–Santonian) and Anambra–Benin phase (Campanian–Mid Eocene). These phases happened as an effect of the uplift of the Abakaliki region (this uplift is confirmed in this study), Santonian folding and depocenter dislocation into the Afikpo region and Anambra block (Murat 1972; Hoque and Nwajide 1985). The subsequent succession includes the Nkporo group, Mamu Formation, Imo Formation and Ameki Group (Fig. 3). The formation of the

petroliferous Niger Delta Basin is linked to the Niger–Delta phase (late Eocene–Pliocene; Oboh-Ikuenobe et al. 2005). Limestone, shale and sandstone constitute the Asu River Group of the Abakaliki formation, and the Calabar formation is comprised mostly of the Mfamosing Limestone (Petters 1982). The estimated thickness of the Awgu Shale is approximately 900 m (Benkhelil 1986).

The crystalline metamorphic rocks of Neo-Proterozoic age (Oban and Bamenda Massifs) are also present in the study area. These rocks are mainly migmatite gneisses, banded gneisses, coarse porphyritic granites, and pegmatites with thin dykes of intermediate–basic intrusive and hyperbysal rocks. They generally underlie the sedimentary fills of the Lower Benue Trough (Oha et al. 2016). A sedimentary sequence of an approximate thickness of 3500 m
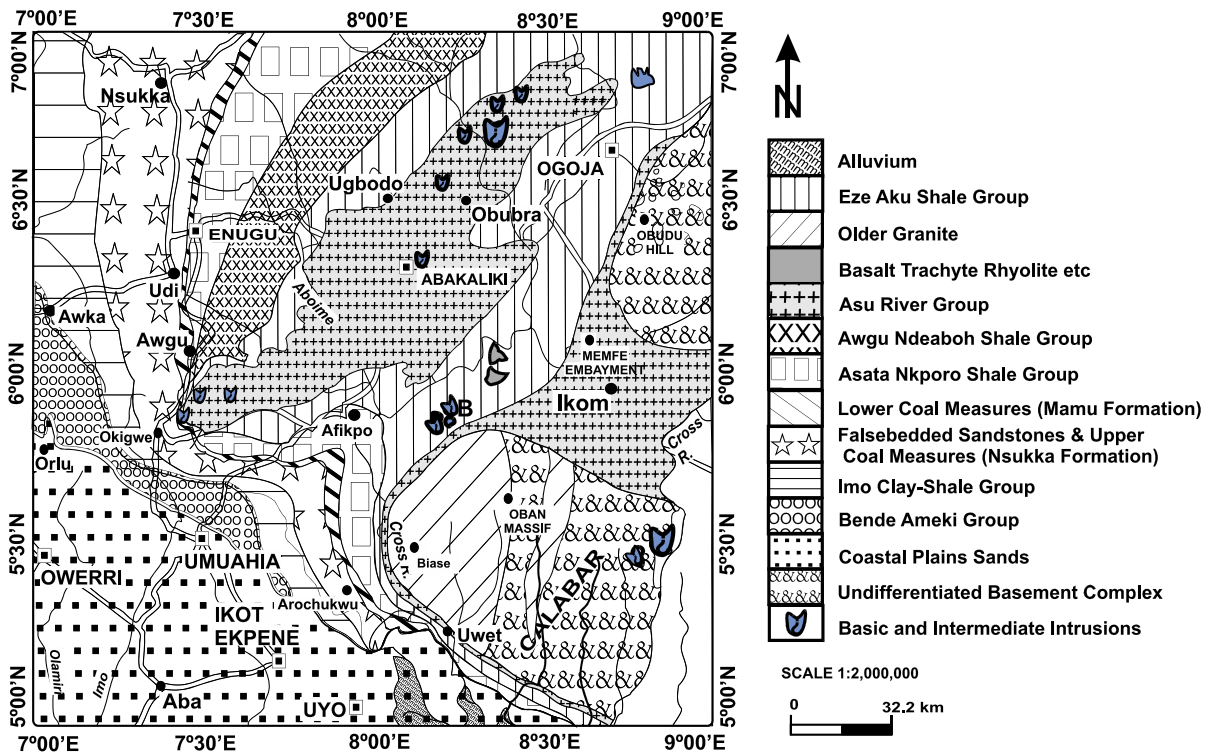
Figure 3
Map of the coverage area showing the geological setting. This map presents detailed geological information on the studied region as selected in Figs. 1 and 2. Locations of the various geologic units show emplacement of igneous rocks in a folded Albian to Turonian sedimentary sequence which consists mainly of calcareous shales with subordinate siltstones, sandstones and occasionally interbedded limestones and mudstones

and consisting of the Nsukka Formation ($\sim$ 350 m), Imo Formation ($\sim$ 1000 m), Ameki Group ($\sim$ 1900 m) and Ogwashi–Asaba Formation ($\sim$ 250 m) stems from the Paleogene time (Oboh-Ikuenobe et al. 2005). Mean thermal conductivity evaluated from various wells drilled for oil exploration on each of the formations by Onuoha and Ekine (1999) indicates high thermal conductivities within Eze-Aku (2.1 Wm^{-1} k^{-1}), Mamu (1.94 Wm^{-1} k^{-1}) and Nsukka (1.83 Wm^{-1} k^{-1}) Formations. Other evaluated formations include: Awgu Shale (1.75 Wm^{-1} k^{-1}), Bende Ameki (1.59 Wm^{-1} k^{-1}), Imo Shale (1.68 Wm^{-1} k^{-1}) and Nkporo Shale (1.55 Wm^{-1} k^{-1}). Average thermal conductivities of 1.80 and 2.5 Wm^{-1} k^{-1} were used for the sedimentary shale formation (Manea and Manea 2011) and for the region with igneous rock (older granite) in our computations of heat flow. Figure 4 summarizes stratigraphic data on the Palaeogene sequence in southeastern Nigeria.

3. Methods

3.1. Magnetics

Combination of magnetic and gravity methods is essential towards presenting a better understanding of the geothermal structure within our study area. Each method probes different rock properties (magnetic susceptibility variations from magnetic data and density variations from gravity data). In geothermal exploration, magnetic measurements generally aim mainly towards locating hidden intrusive bodies and estimating their depths, as well as tracking individual buried dykes and faults. They can also enable location of regions with reduced magnetization due to thermal activity (Georgsson 2009). Our analysis of aeromagnetic data is used to produce a contoured CPD map. This map representation should correlate to a significantly higher extent with various known indicators of geothermal activity in the region under
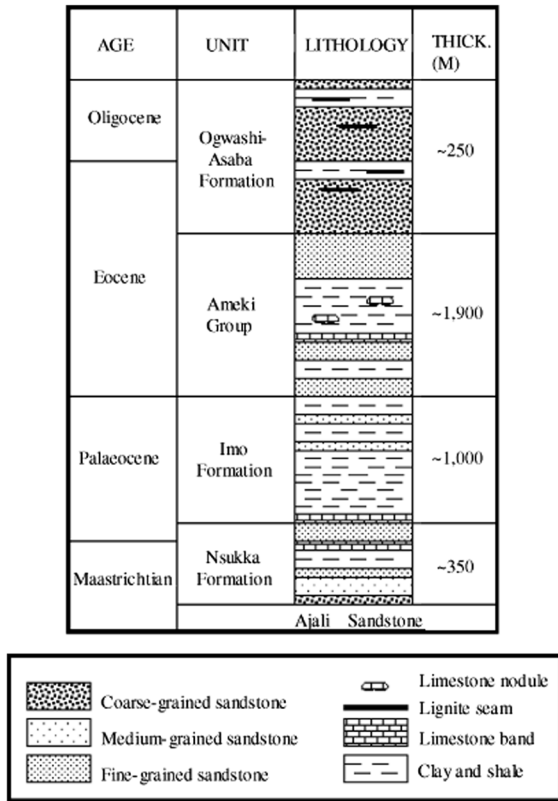
Figure 4
Stratigraphic data on the Paleocene succession in southeastern Nigeria (modified from Oboh-Ikuenobe et al. 2005). The estimated formation thickness of the various formations is portrayed on the figure

consideration (Bansal et al. 2011). The manner in which the depth range of magnetic sources is determined could be grouped into those examining the shape of isolated magnetic anomalies (e.g. Bhattacharyya and Leu 1975) and those considering statistical characteristics of patterns of magnetic anomalies (e.g. Spector and Grant 1970). By transforming the spatial data into frequency domain, both techniques present the connection that exists between the spectrums of magnetic anomalies and depth of magnetic sources (Tanaka et al. 1999; Obande et al. 2014). CPD investigations were determined for some parts of Japan (Okubo et al. 1985, 1994), USA (Blakely 1988; Mayhew 1985), Portugal (Okubo et al. 2003), Greece (Stampolidis and Tsokas 2002; Tsokas et al. 1998), India (Rajaram et al. 2009; Bansal et al. 2013), Bulgaria (Trifonova et al. 2006, 2009), Turkey (Dolmaz et al. 2005; Maden

2009), Mexico (Manea and Manea 2011) and Nigeria (Obande et al. 2014; Abraham et al. 2014, 2015; Chukwu et al. 2018). The power spectrum of the total geomagnetic anomaly field was considered on a single rectangular block first proposed by Bhattacharyya and Morley (1965). A major result of Spector and Grant's analysis presents the expectation value of the spectrum being same as that of a single body with the average parameters for the collection (Okubo et al. 1985). For the magnetic data analysis, we follow the procedures of Okubo et al. (1985) and Tanaka et al. (1999). The top bound and the centroid of a magnetic source, z_t and z_o, respectively, are calculated from the power spectrum of magnetic anomalies and utilized to estimate the basal depth of a magnetic source z_b. From the assumptions that 1) the layer extends infinitely far in all horizontal directions, 2) the depth to the top bound of a magnetic source is small compared with the horizontal scale of a magnetic source, and 3) magnetization $M(x, y)$ is a random function of x and y, the power density spectra of the total field anomaly $\Phi_{\Delta T}$ (Blakely 1995; Tanaka et al. 1999):

$$\Phi_{\Delta T}\left(k_x, k_y\right) = \Phi_M\left(k_x, k_y\right) \times F\left(k_x, k_y\right)$$

$$F\left(k_x, k_y\right) = 4\pi^2 C_m^2 |\Theta_m|^2 |\Theta_f|^2 e^{-2kz_t}(1 - e)^2 \quad (1)$$

where Φ_M is the power-density spectra of the magnetization, C_m is a proportionality constant, and Θ_m and Θ_f are factors for magnetization direction and geomagnetic field direction, respectively. This equation can be simplified by noting that all terms, except $|\Theta_m|^2$ and $|\Theta_f|^2$, are radially symmetric. Moreover, the radial averages of Θ_m and Θ_f are constant. If $M(x, y)$ is completely random and uncorrelated, $\Phi_M\left(k_x, k_y\right)$ is a constant. Hence, the radial average of $\Phi_{\Delta T}$ is:

$$\Phi_{\Delta T}(|k|) = A e^{-2kz_t} \left(1 - e^{|-k(z_b - z_t)|}\right)^2 \quad (2)$$

where A is a constant. For wavelengths less than about twice the thickness of the layer, Eq. 2 approximately becomes:

$$\ln\left[\Phi_{\Delta T}(|k|)^{1/2}\right] = \ln B - |k|z_t \quad (3)$$

where B is a constant. Using the slope of the power spectrum, one could estimate the top bound of a

magnetic source. On the other hand, Eq. 2 rewrites as:

$$\Phi_{\Delta T}(|k|)^{1/2} = C\mathrm{e}^{-kz_t - z_o}\left(\mathrm{e}^{-k()k(z_t - z_o)} - \mathrm{e}^{-k(z_b - z_o)}\right)$$

(4)

where C is a constant. At long wavelengths, Eq. 4 is:

$$\Phi_{\Delta T}(|k|)^{1/2} = C\mathrm{e}^{-kz_o}\left(\mathrm{e}^{-k(-d)} - \mathrm{e}^{-k(-d)}\right) \sim C\mathrm{e}^{-kz_o}2|k|d$$

(5)

where $2d$ is the thickness of the magnetic source. From Eq. 5

$$\ln\left\{\left[\Phi_{\Delta T}(|k|)^{1/2}/|k|\right]\right\} = \ln D - |k|z_o \qquad (6)$$

where D is a constant. We summarize Eqs. (3) and (6) as

$$\ln\left[P(k)^{1/2}\right] - \ln B - |k|z_t \qquad (7)$$

and

$$\ln\left[P(k)^{1/2}/|k|\right] - \ln D - |k|z_o \qquad (8)$$

where $\Phi_{\Delta T}(|k|)^{1/2}$ is written as $P(k)^{1/2}$.

We estimated the top bound and the centroid of the magnetic source by fitting a straight line through the high wavenumber and low-wavenumber parts of the radially averaged spectrum of $\ln\left[P(k)^{1/2}\right]$ and $\ln\left[P(k)^{1/2}/|k|\right]$ from Eqs. (7) and (8) respectively. As our frequency unit is in cycles per kilometer, we divided the corresponding spectrum relation by (4π). The depth to bottom (basal depth) of the magnetic source is given by:

$$z_b = 2z_o - z_t \qquad (9)$$

CPD is assumed as the obtained basal depth computations (Okubo et al. 1985; Tanaka et al. 1999).

3.2. Conductive Heat Flow

A fundamental relation when considering conductive heat conveyance is Fourier's law (Tanaka et al. 1999). In the one-dimensional case, assuming a vertical direction for temperature variation and constant temperature gradient $\mathrm{d}T/\mathrm{d}z$, Fourier's law takes the form

$$q = k\frac{\mathrm{d}T}{\mathrm{d}z} \qquad (10)$$

where q is described as the heat flux and k is the coefficient of thermal conductivity.

The Curie temperature (θ) can be defined as:

$$\theta = \left(\frac{\mathrm{d}T}{\mathrm{d}z}\right)z_b \qquad (11)$$

where z_b is the CPD, provided that there is no heat sources or heat sinks between the Earth's surface and the CPD, the surface temperature is 0 °C and $\mathrm{d}T/\mathrm{d}z$ is constant.

Any given depth to a thermal isotherm is inversely proportional to heat flow as demonstrated by Tanaka et al. (1999). Heat flow and geothermal gradient values were calculated using Eqs. (10) and (11) and were based on CPD estimates realized from the magnetic computations. We utilize the Curie point (θ) for magnetite (580 °C with an average thermal conductivity of 1.80 $\mathrm{Wm}^{-1}\,\mathrm{k}^{-1}$ (Onuoha and Ekine 1999) for the sedimentary shale formation and 2.5 $\mathrm{Wm}^{-1}\,\mathrm{k}^{-1}$ (Manea and Manea 2011) for the region with igneous rock (older granite).

3.3. Gravity

Gravity surveys are very valuable in conventional hydrothermal system exploration as they can be used to identify subsurface anomalies connected with deep granitic and magmatic bodies including zones of alteration and fault structures indicative of geothermal activities. Such zones have density contrast with the surrounding unchanged rock. Fault structures provide preferential pathways through the subsurface for the circulation of geothermal fluids and in many cases, these fault structures are concealed by younger sedimentary cap rock succession (Kohrn et al. 2011). Gravity analysis has proven successful for the discovery of such concealed geothermal systems. Gravity studies (Montesinos et al. 2003; Gottsmann et al. 2008; Kohrn et al. 2011; Represas et al. 2013;

Mohammadzadeh-Moghaddam et al. 2016) have demonstrated the possibilities of achieving practical results for geothermal exploration, which includes delineation of faults and fracture regions analogous to the reservoir of geothermal system, probing of basement configurations in a geothermal area (Salem et al. 2005; Soengkono 2011; Nishijimaa and Naritomi 2017) and magma chambers and intrusive bodies related to the heat source of a geothermal system (Represas et al. 2013). Gravity and magnetic methods present the most economical geophysical techniques to obtain an acceptable model for a geothermal system (Mohammadzadeh-Moghaddam et al. 2016). In our gravity data analysis, we shall apply edge detection filters: the tilt derivative (TD) and the improved normalized horizontal (INH) tilt angle evaluation (Li et al. 2014; Nishijimaa and Naritomi 2017). Enhancement of the edges of causative sources is a universal tool in the interpretation of potential field data. Many of the existing balanced edge detection filters of potential field data only use the feature that the vertical derivative is zero above the source edges to recognize the source edges and this produces spurious edges in the interpretation (Li et al. 2014). The INH as proposed by Li et al. (2014) gives maximum values when the horizontal derivative reaches their maximum values and the vertical derivatives become zero, it does not produce spurious edges and provide more accurate results. In addition, the effect of noise is suppressed and edges are displayed more clearly compared to previous edge detection filters.

The total horizontal derivative (THD; Miller and Singh 1994; Thurston and Smith 1997; Verduzco et al. 2004) maximizes above any abrupt change of density and for grids, it is given by (Cordell and Grauch 1985; Nishijimaa and Naritomi 2017):

$$\text{THD} = \sqrt{\left(\frac{\partial g}{\partial x}\right)^2 + \left(\frac{\partial g}{\partial y}\right)^2} \qquad (12)$$

where $(\partial g/\partial x)$ and $(\partial g/\partial y)$ are the directional derivatives of the gravity anomaly in the x and y directions, respectively. The advantage of the THD is that it is less susceptible to noise and can reorganize the edges of both shallow and deep structures clearly.

The INH tilt angle filter is given as:

$$\text{INH} = \tan^{-1}\left(\frac{\sqrt{\left(\frac{\partial g}{\partial x}\right)^2 + \left(\frac{\partial g}{\partial y}\right)^2}}{p + \left|\frac{\partial g}{\partial z}\right|}\right) \qquad (13)$$

where p is a positive constant value and is decided by the interpreter. In general, the value of p is approximately equal to one-tenth or one-twentieth of the maximum of the THD (Li et al. 2014).

We estimated crustal thickness (depth to Moho) from gravity data assuming a single density contrast within the crust and its base (Moho). Riad et al. (1981) and Bilim (2007) propose the relation between the thickness of the crust and gravity anomalies:

$$H = 29.98 - 0.075\Delta g \qquad (14)$$

where H is thickness of the crust in kilometers and Δg is the gravity anomaly values in mGal.

4. Data Analysis and Results

4.1. Aeromagnetic Data

Aeromagnetic survey over the study area was conducted under the auspices of the NGSA between years 2005 and 2009. Data was acquired using a mean terrain clearance of 80 m and 500-m line spacing. The geomagnetic gradient was eliminated from the aeromagnetic data using the International Geomagnetic Reference Field (IGRF) formula of 2005. We used data reduced to the equator (RTE) in our analysis of the magnetic data. Baranov (1957) described a technique known as reduction to the pole (RTP) for reducing the magnetic maps made anywhere, except at very low latitudes, to their expected nature, assuming inclination of the magnetic field were 90° (Jain 1988). Although the RTP technique has seen some refinements and methods of execution over the years, Leu (1981) proposed the RTE technique and demonstrated that the RTE technique was more reliable at high latitudes than the RTP technique is at low latitudes. Jain (1988) compared the RTP with RTE techniques and concluded that the RTE technique is preferable, more particularly at the middle and lower latitudes. Given the location of our study area (lower latitudes), we applied the RTE correction assuming a magnetic declination

of $-2.15°$ and an inclination of $-13.91°$ for the study area utilizing the fast Fourier transform operator. To remove the effects of topography on the aeromagnetic anomalies, the RTE data were low-pass-filtered using a cutoff wavenumber of $0.98~km^{-1}$ adopted from the point of change of the short and long wavenumber segments of the power spectrum of the whole data. Figure 5 shows the resulting RTE geomagnetic field map of the study area. Positive anomalies ranging between 90 and 170 nT are noticeable around the Enugu–Udi–Agwu streak. These anomalies could be traced to the lower coal measures of the Mamu Formation. Positive anomalies of 120–200 nT noticed within the Okigwe–Umuahia area are traced to subsurface basic and intermediate intrusions within the area with some exposures around Okigwe within the Asu River Group. Other notable anomalies ranging between 270 nT and 400 nT are observed around the Biase locality and are traced to response within the older granite of the undifferentiated basement complex. In the same vein, negative anomalies ranging from -20 to -370 nT are observed southwards of Biase town within the Coastal Plain Sands and northwards of Obubra within the Asu River and Eze Aku Shale Formations. It was generally observed that the undifferentiated basement complex of the Oban Massif and Obudu Hill gave positive magnetic responses of within 5–350 nT.

The estimation of CPD is executed basically in two steps: the first is to calculate the z_t of depth to the top of magnetic sources using Eq. (7) and the second is to calculate z_o representing depths to the centroid of magnetic sources using Eq. (8). A concession between the spatial resolution and safeguarding the long-wavelength part of the spectrum is called for in the decision on the block sizes to be used. A number of assumptions and problems are associated with estimation of the CPD. Uncertainties about the nature of magnetization depth affect assumed Curie temperatures, and the basal depth itself may be caused by a lithological contact rather than a thermal boundary. Given the complexity of the geological setup in the region, we assume a random and uncorrelated magnetization in our investigation. The magnetization of an extrusive volcanic layer, for example, may have different statistical properties from plutonic rocks (Blakely 1988; Aboud et al. 2011; Ross et al.

2006). Further, regional-scale magnetic anomaly databases (as used in our study) are usually composed of a mosaic of individual aeromagnetic surveys. Owning to differences in survey specifications, subtle discontinuities can occur along survey boundaries. These discontinuities can contribute long wavelength noise to the regional compilation and may contaminate long wavelength signals caused by deep magnetic sources (Ross et al. 2006; Aboud et al. 2011).

Notwithstanding the achievement of an accurate z_b using the technique, there is no assurance that z_b portrays the Curie temperature depth. Other geologic explanations unrelated to crustal temperatures abound for truncated magnetic sources (Trifonova et al. 2009). Deep magnetic sources have long wavelengths and low amplitudes, which makes them difficult to distinguish from anomalies caused by shallow sources. The dimension of the subregion must be sufficiently large to capture these long wavelengths, thus forcing a trade-off between accurately determining z_b within each subregion and resolving small changes in z_b across subregions (Ross et al. 2006).

In selecting our block size, an effort was made to follow the suggestion by Shuey et al. (1977) to consider information on spectrum depth to instruct on window lengths chosen. The depth resolution is limited to the length of the aeromagnetic profile (L) and the maximum CPD estimation is limited to $(L)/2\pi$ (Shuey et al. 1977; Manea and Manea 2011). For source bodies having bases deeper than $L/2\pi$, the spectral analysis procedure might not be viable (Salem et al. 2000). We divided the magnetic anomaly map into subregions of dimension 110×110 km ensuring that the blocks overlapped by 50% of the block size. We then sampled additional blocks placing center points of subregions within notable geologic provinces following Ross et al. (2006) and Abraham et al. (2015). This was done to capture and emphasize magnetic anomalies associated with each province. A total of 14 blocks were obtained using the 110×110-km dimension. The statistical errors for each of the selected windows were computed from the standard deviation of differences between the natural logarithm of power density spectrum and the linear fit from the least square method. The range of frequencies considered for these evaluations were
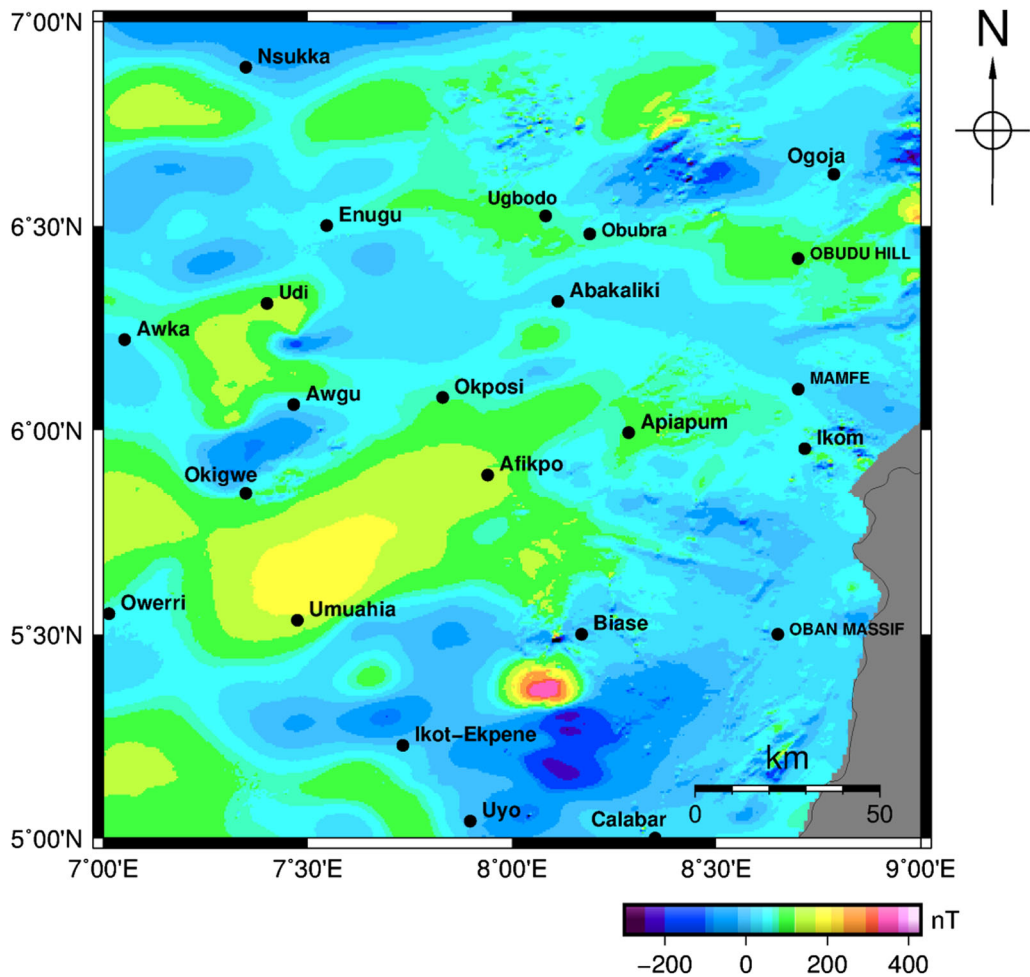
Figure 5
Geomagnetic anomaly map of the coverage area. The data were reduced to the equator using a declination of −2.15° and an inclination of −13.91° for this region. The map shows significant positive anomalies in the central and southwestern regions of Afikpo and Umuahia, indicating stronger magnetic field presence in these regions. Negative (weaker) anomalies are also perceptible at the southern regions of Uyo–Calabar and northern regions of Abakaliki–Ogoja

taken within the range of the linear fits on each spectrum. This technique has been successfully applied by Okubo and Matsunaga (1994), Trifonova et al. (2009); Manea and Manea (2011) and Abraham et al. (2014). Figure 6 shows an example of the radially averaged power spectrum plot for block number 8. From the centroid depth of 7.86 ± 0.01 km and depth to the top of 0.52 ± 0.04 km, CPD is calculated as 15.21 ± 1.18 km. Table 1 display results of spectral analysis and depth estimations of magnetic sources including error estimations for the selected blocks.

Figure 7 display the map of estimated CPDs for the study area.

4.2. Gravity Data

Satellite-derived gravity anomaly data (Sandwell and Smith 2009; Sandwell et al. 2013, 2014) was used for our analysis. The gravity data is dependent on the resource of a new radar altimetry data sets (CryoSat-2 and Jason-1) with high track density. Their newer radar technology results in a 1.25-times improvement in range precision that maps directly
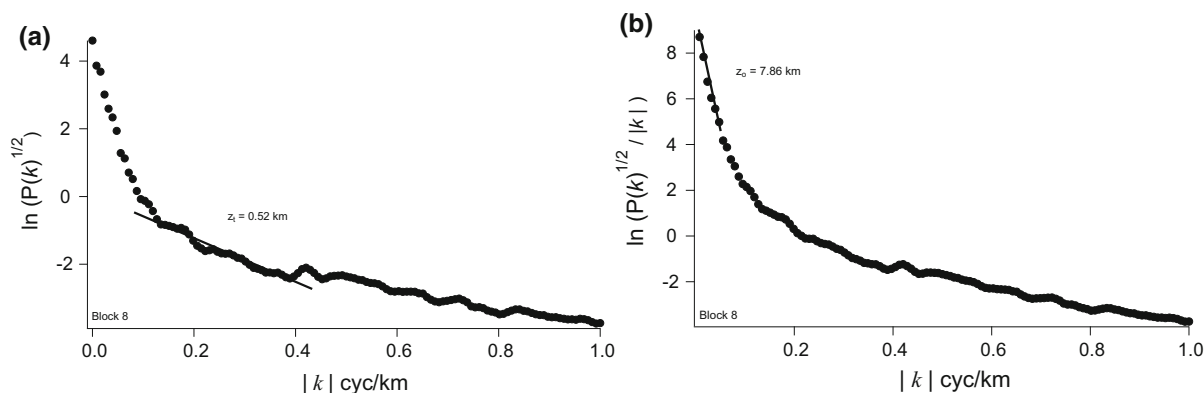
Figure 6

Illustration of radially averaged power spectrum on block 8. **a** A value of 0.52 km is estimated depth at the top and **b** estimates a value of 7.86 km as the centroid depth. The gradients of spectra, defined as $\ln\left[P(k)^{1/2}\right]$ and $\ln\left[P(k)^{1/2}\right]/|k|$, where $|k|$ is the wavenumber and $P(k)$ is the radially averaged power spectrum, were used on both occasions. The resulting z_b computed for this block is 15 ± 1.18 km

Table 1

Spectral analysis results with depth estimations of magnetic sources. Error estimations on the results are also shown

Block	Location		z_t (km)	Error z_t ($\pm$ km)	z_o (km)	Error z_o ($\pm$ km)	CPD (km)	Error CPD ($\pm$ km)
	Longitude, X	Latitude, Y						
1	7°30′	5°30′	0.439	0.046	7.409	0.228	14.38	2.39
2	7°59′	5°31′	0.375	0.010	9.686	0.559	18.99	2.72
3	7°59′	6°29′	0.394	0.012	8.907	0.175	17.42	1.23
4	7°59′	5°59′	0.407	0.013	9.424	0.171	18.44	1.25
5	8°30′	5°31′	0.401	0.016	8.049	0.160	15.70	1.25
6	8°29′	5°59′	0.395	0.036	7.963	0.092	15.53	1.78
7	8°29′	6°29′	0.439	0.031	5.106	0.239	9.77	1.60
8	7°30′	6°29′	0.516	0.038	7.863	0.012	15.21	1.18
9	7°30′	5°59′	0.589	0.038	8.618	0.035	16.65	1.20
10	8°14′	6°23′	0.421	0.027	6.479	0.165	12.54	1.44
11	7°44′	5°47′	0.424	0.016	9.877	0.317	19.33	1.98
12	7°34′	6°17′	0.462	0.019	8.345	0.181	16.23	1.38
13	7°53′	5°40′	0.349	0.014	8.797	0.311	17.25	1.91
14	8°20′	6°29′	0.415	0.030	6.317	0.235	12.22	1.80

into gravity field improvements. The observations were conducted with common global 1-min grids, and the error of gravity data computation was estimated at 1.5–2 mGal. These gravity data are of superior quality compared to a majority of publicly available academic and government ship gravity data (Sandwell et al. 2013). Developments in airborne gravitational studies yield large amounts of data, which can be used to model the subsurface with a relatively high level of accuracy (Manzella 2009).

Authors (Mishra et al. 2012; Eppelbaum and Katz 2015a, b, 2017) have demonstrated the high effectiveness of satellite-derived gravity data for delineation of different tectono-structural units. We obtain free-air (FA) anomaly and topography data from Sandwell and Smith (2009) and Sandwell et al. (2013, 2014) to cover the region of our study. This data was gridded at 500-m grid spacing using the minimum curvature method and the results presented in Fig. 8. The FA anomaly map shows segmentation
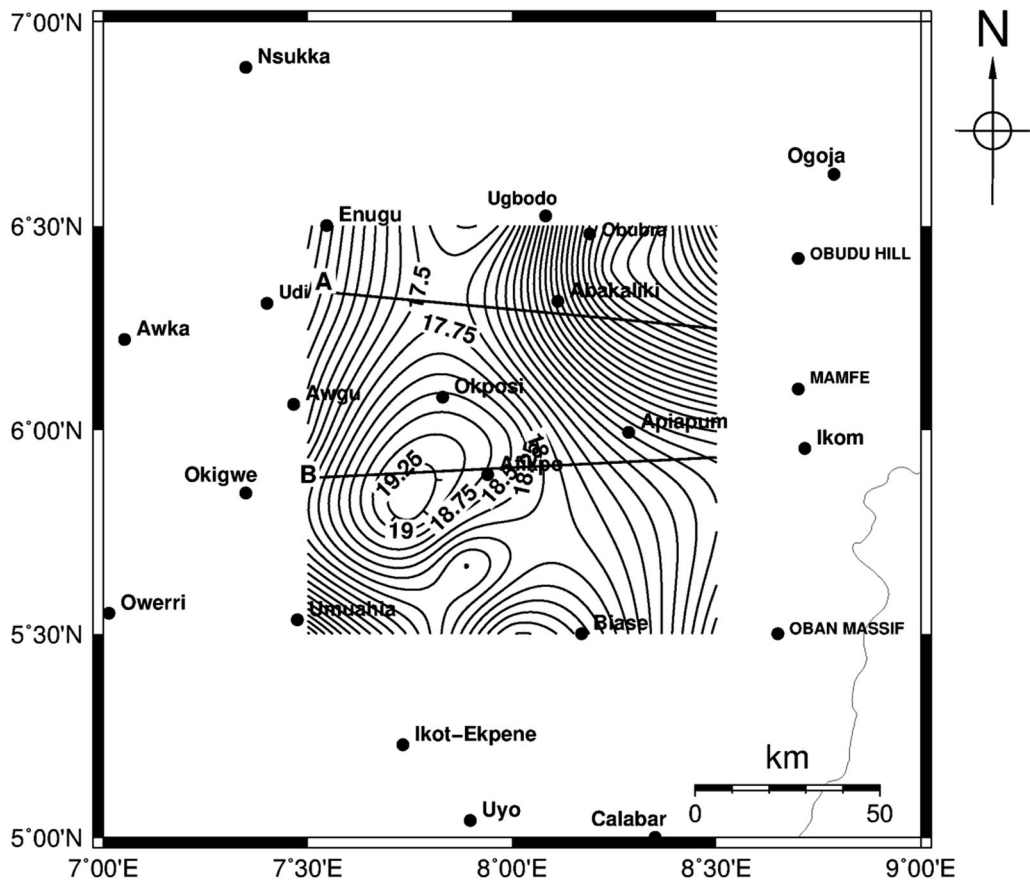
Figure 7

CPD map results for the coverage area. Depths were computed using two-dimensional spectral analysis of the anomaly data using 14, 50% overlapping square blocks. Profiles A and B represent profiles taken across significant CPD regions in order to examine depth sections and subsurface structural interaction in the region. The profiles were used to analyze interactions of the depth to the top, depth to the centroid, and CPD from magnetic data analysis and compared with the estimated depths to the Moho from gravity data as presented in Fig. 11

of positive gravity anomalies. Gravity highs are seen at the NW and SE regions of the map, sandwiching a NE–SW-trending gravity low. We envisage that the gravity high at the SE region could be due to high-density intrusions in the crystalline complex. That of the NW region could be due to some high-density intrusion within the shale formation in the area.

From the FA anomaly data obtained (Fig. 8), we computed the complete Bouguer anomaly for the region using an Earth density of 2.67g/cm³. The complete Bouguer anomaly amends the Bouguer anomaly for lack of regularity of the Earth as a result of the terrain in the vicinity of the observation point. We perform a regional-residual field separation on the complete Bouguer anomaly data using the least

square best-fit polynomial technique and gridded the residual output with 500-m grid spacing. Figure 9 shows the residual complete Bouguer anomaly map realized from the computation with superimposed geologic features of the region. The super-positioning of the geological map was performed to assess the conformity of the geologic units to structural features on the complete Bouguer anomaly map. All subsequent analyses were performed on the residual complete Bouguer anomaly data.

Figure 9 correlates in a good manner with the geological map of the coverage area. The responsiveness of gravity method to the distribution of geologic materials in the subsurface with varying densities has proven value in geothermal exploration.
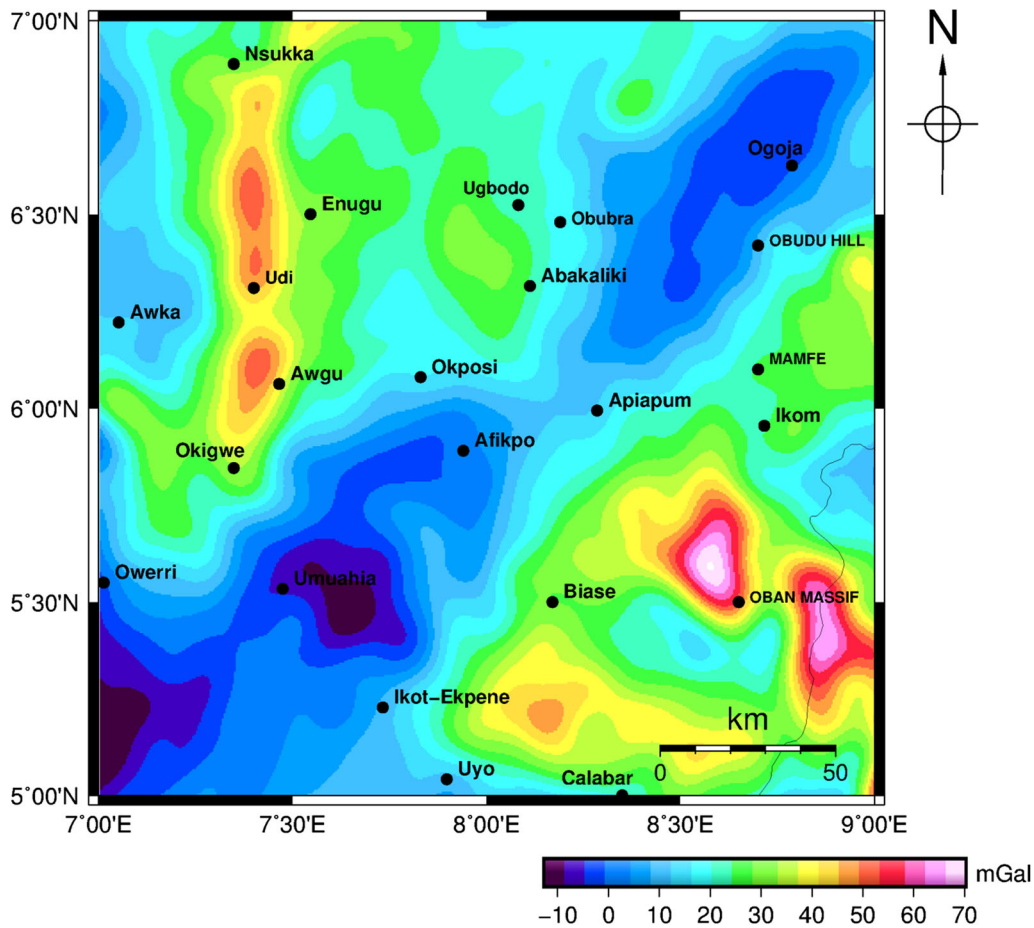
Figure 8

Free-air gravity anomaly data from Sandwell et al. (2013, 2014). The satellite-derived gravity data were obtained with common global 1-min grids, and the error of gravity data is estimated at 1.5–2 mGal. The map shows significant positive anomalies at Nsukka, Udi and Awgu regions located on the false bedded sandstones and the Upper coal measures (Nsukka Formation). The southeastern region of the study area also shows positive anomalies from the older granite unit at the Uban Masiff position. Negative anomalies are also observed running NE–SW across the study area

A feature with high density within a low-density medium should present a positive Bouguer anomaly and features with low densities within a higher-density medium should give rise to negative Bouguer anomalies (Rivas 2009). The thickness of the crust (Moho) was computed from the residual complete Bouguer anomaly map and results are displayed in Fig. 10. CPD results (Fig. 7) were superimposed on Fig. 10 to analyze their relationship with respect to the tectonic events in the region.

To further understand the subsurface interactions with respect to the estimated depths (deeper and shallow), we use profiles (profiles A and B) across the

regions ensuring that each profile cuts across notable depth anomalies in the study area (Fig. 7). We evaluated the subsurface structure considering topography, depth to the top, centroid and basal (assumed CPD), and Moho (computed from the complete Bouguer anomaly data). Results from this evaluation are presented in Fig. 11.

We superimpose the faults obtained from the analysis of gravity data (Fig. 12) and the inferred faults from the lineament map (Fig. 2) on the CPD results in order to examine intercalations of faults structures for realistic geothermal prospects in the region and further compare the tectonic relations as
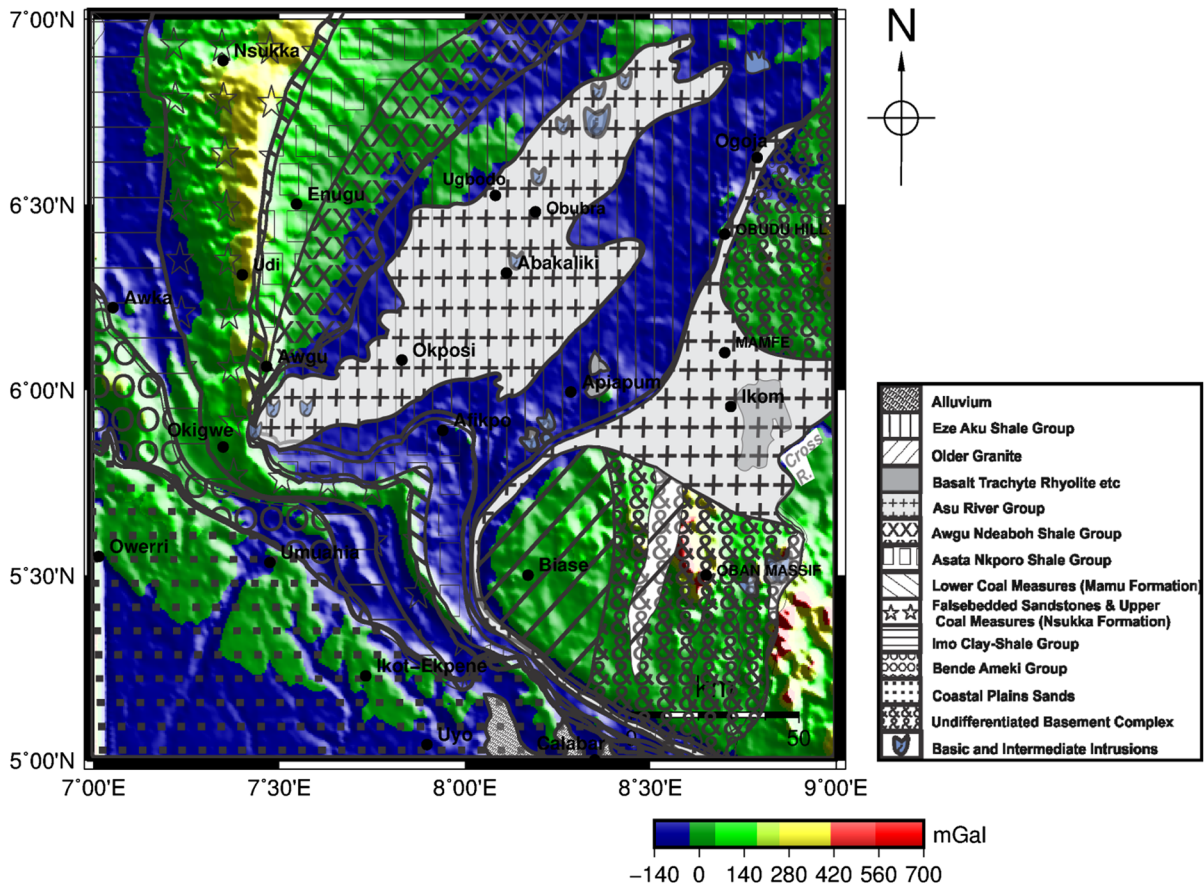
Figure 9
Residual complete Bouguer anomaly map of the coverage area with a superimposed geological map. The super-positioning allows examination of the correlation between the main geologic features in the region (Fig. 3). A useful correlation is achieved as most of the geologic boundaries have been mapped by the complete Bouguer anomaly

regards the estimated CPD. The result is displayed in Fig. 13.

We present results from the edge detection filter (INH) applied to the complete Bouguer anomaly data (Fig. 9) in Fig. 14 below.

5. Discussion

We discuss pioneering results achieved from our study in the following explanatory notes. The estimated CPDs in Fig. 7 show deeper depth results within an approximate range of 18 and 20 km towards the central and southern regions of the map (Okposi, Afikpo and Biase regions). Shallow depths within an approximate range of 9 and 17 km have

also been estimated for the Ugbodo, Obubra and Ababaliki locations, NE of the study area. General appraisal shows that a minimum depth of 9.77 ± 0.73 km and maximum depth of 19.33 ± 0.95 km with an average value of 15.69 ± 0.86 km were estimated for the study area. The deeper depths around the Afikpo region are related to the structural inversion of the Benue Trough that led to the subsidence of the Afikpo syncline (Fig. 3). Deeper CPDs around the Enugu–Okposi–Afikpo axis could be associated with the depocenters of the Lower Benue Trough. The depocenters within the Anambra Basin are found within Enugu, Awka and Okigwe (Obaje 2009). We attribute the shallow CPDs obtained around Ugbodo, Obubra and Ababaliki regions to the basaltic and doloritic intrusive rock in the region. Some of these
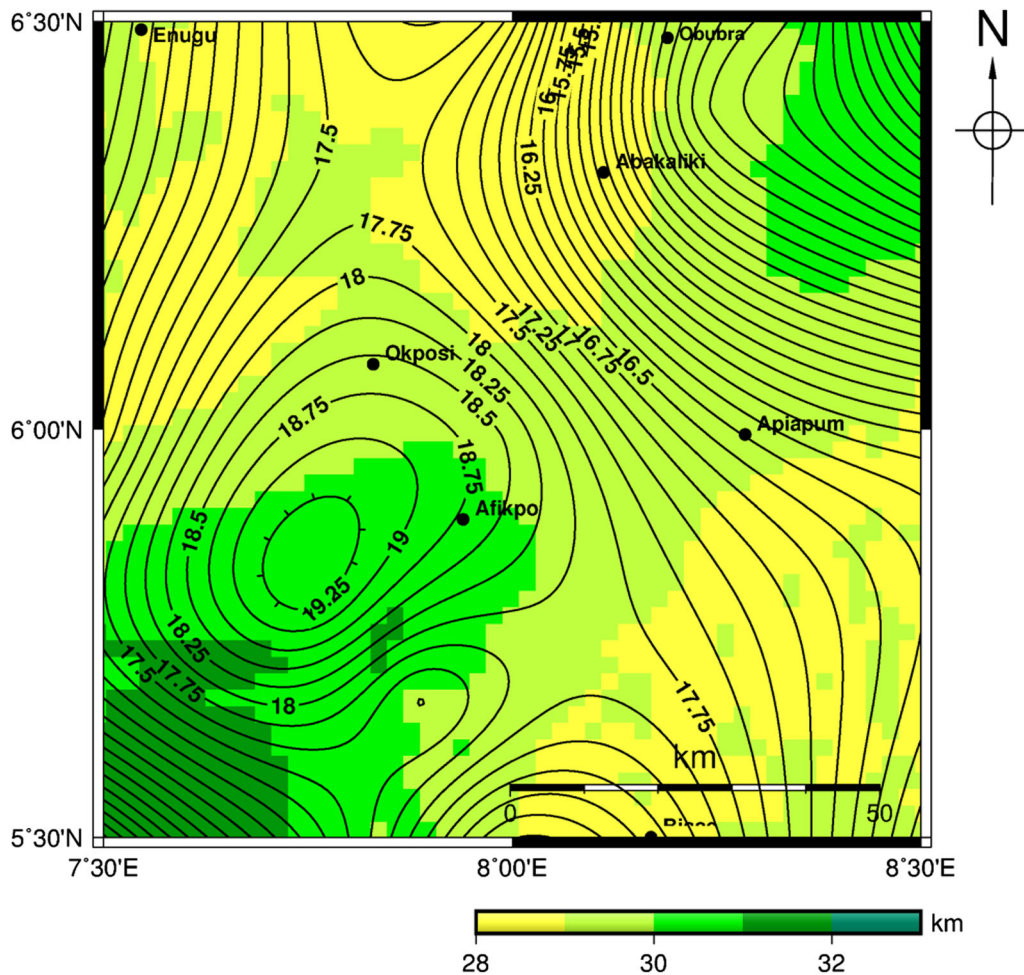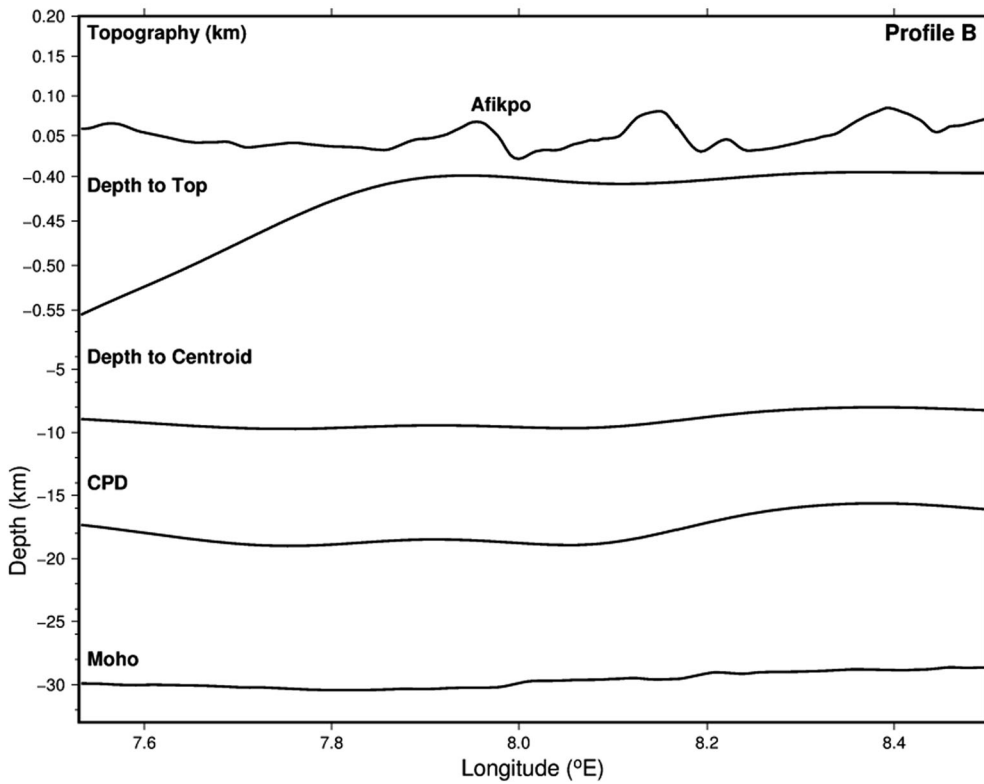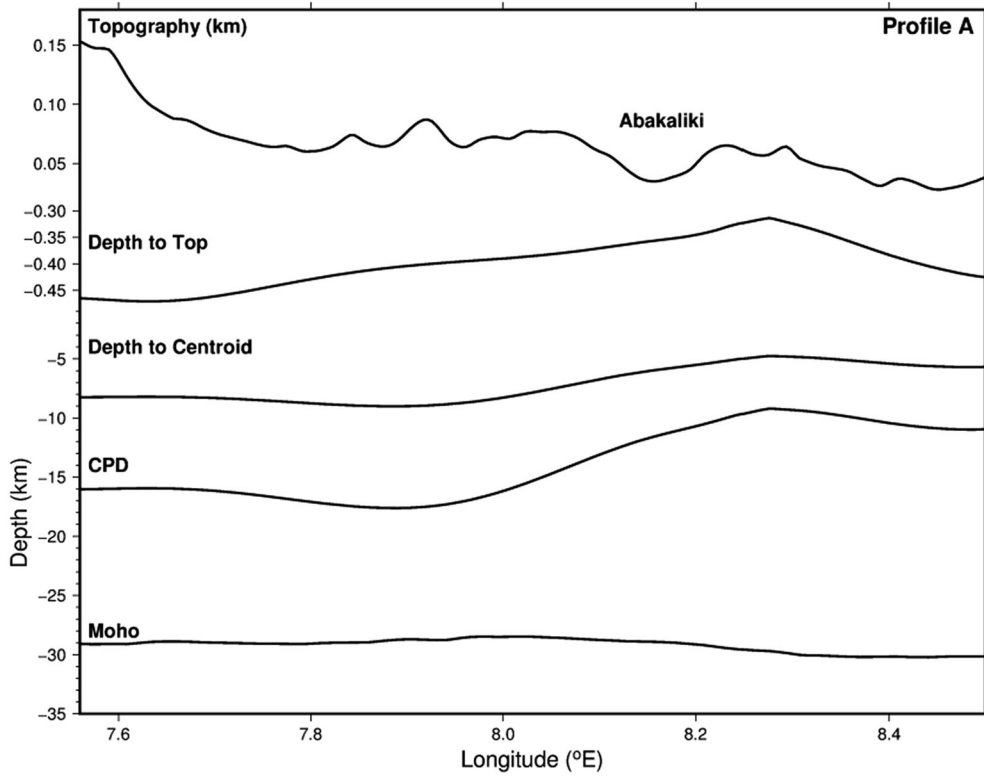
Figure 10

Moho depth results with superimposed CPD results. Some degree of positive correlation is obtained between the Moho and CPDs. Deeper Moho depths are realized at regions with deeper CPDs at Afikpo and parts of the northeast region. Shallow Moho depth obtained at Abakaliki also coincides with the shallow CPDs estimated for the location

intrusions are traced on the geological map of Fig. 3. This region is located northwards of the Abakaliki Anticlinorium and is of the Asu River Group formation, believed to have been formed during the Santonian. It has been proposed that crustal instability and tectonic events during the Santonian were accompanied by wide-spread magmatism, faulting and folding, ultimately resulting in the formation of the Abakaliki Anticlinorium (Kogbe and Obialo 1976). These events in the late Santonian were accompanied by pronounced igneous activities accounting for the occurrence of a large number of intermediate and basic intrusions in the Asu River

Group. We propose that parts of these subsurface intrusions could be responsible for the lower CPDs obtained in our calculations. We also wish to advise caution on the general consideration of our estimated CPD. The obtained CPD is an average for the area and may not resolve local thermal anomalies as observed by Manea and Manea (2011). Another consideration is the complexity of the geology in the region (Fig. 3). Constituents of some windows selected may be non-magnetic, and the magnetic bottom for this case could have reflected the bottom of intruded plutonic rocks in the region and not CPD. This observation is suspected for the Afikpo region

◄Figure 11
Profile shown topography, depths to the top, centroid, CPD, and
Moho. The profiles are marked in Fig. 7. The relationship of the
various estimated depths is shown on the profile plots with shallow
Moho and CPDs confirmed in the Abakaliki region and deeper
depths in the Afikpo region. A thicker magnetic layer is observed
on profile B compared to the thin magnetic layer (due to uplifts) at
the Abakaliki location

(Figs. 3 and 7). It is also possible that shallow CPDs
at Abakaliki–Obubra regions could represent the
bottom of the volcanic rocks in the region. In their
analysis of the tectonomagmatic origin of some vol-
canic and subvolcanic rocks in our study area, Obiora

and Charan (2010) identified basaltic and doloritic
sill structures including volcanic intrusives at the
Abakaliki region. Shallow CPDs are generally char-
acteristic of volcanic arcs (Manea and Manea 2011).
We add that the CPD results may also represent a
vertical change in lithology, such as a subhorizontal
detachment fault or unconformity as shown in
Figs. 2, 3, 12 and 13. The spectral analysis method
may find the CPD at a contact between young vol-
canic rocks overlying a thick section of a weakly
magnetic sedimentary rocks even though the CPD
lies at greater depths (Ross et al. 2006).

Given that this study is the first in the region to
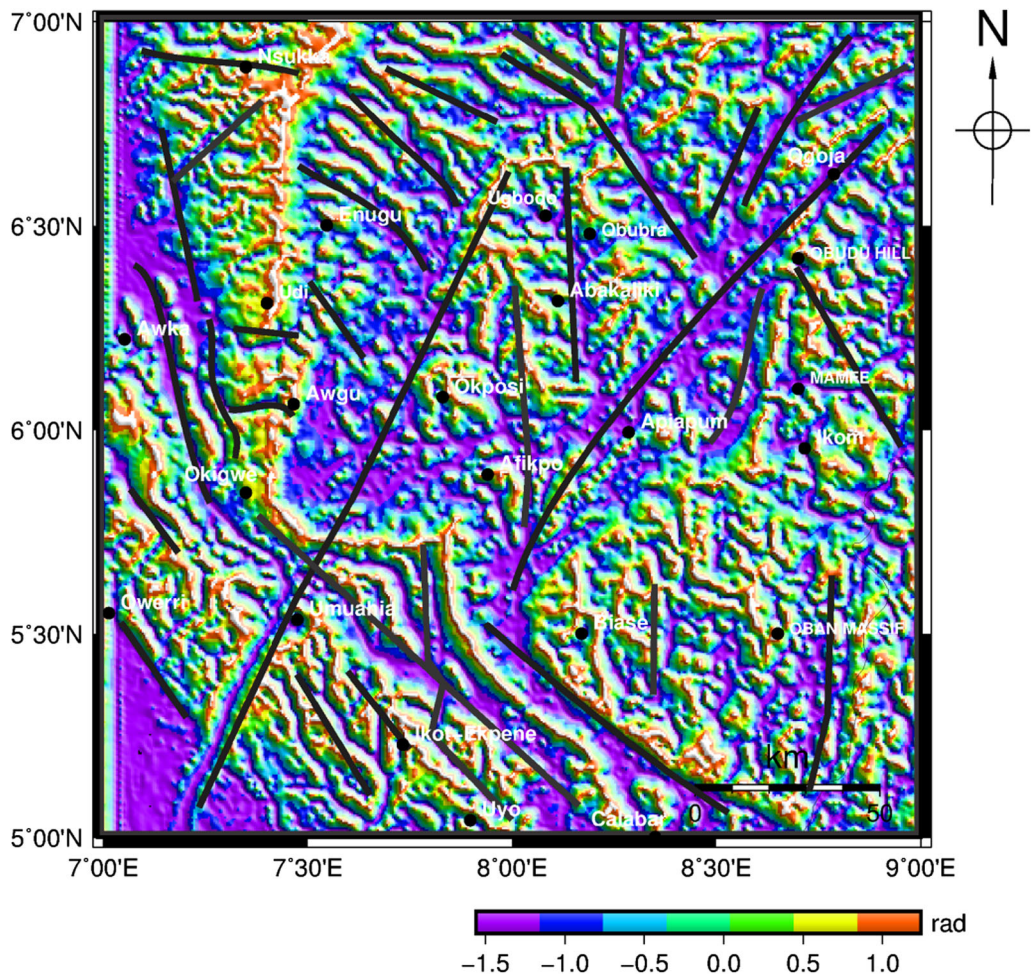evaluate geothermal properties of the subsurface,

Figure 12
Tilt derivative map of the coverage area. The computation was performed on the residual complete Bouguer anomaly data (Fig. 9). Various
trends of lineation could be traced on the map which could indicate faults or lithological contacts
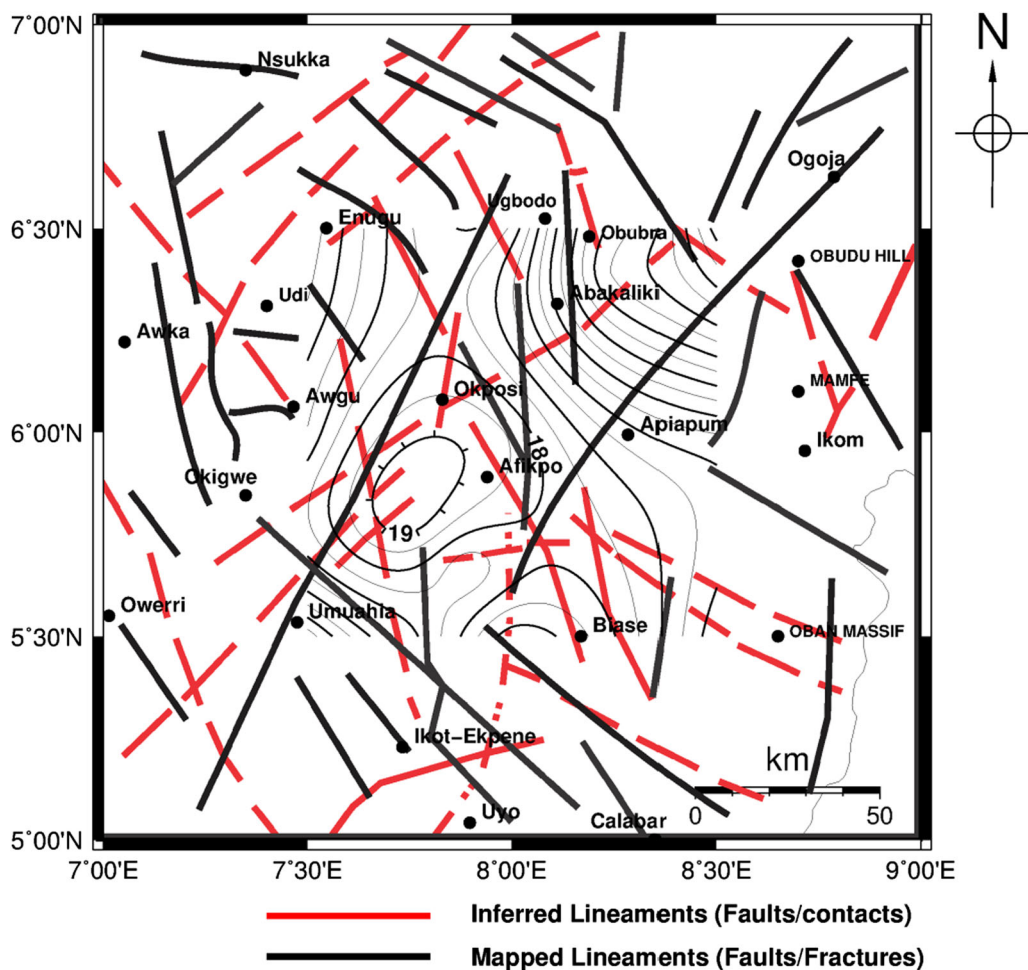
Figure 13

Lineament structure in the study area. These structures were traced from the tilt derivative map (black lines) of Fig. 12 and fault trends from the tectonic representation in Fig. 2 (red lines). We noticed the presence of faults within the region of shallow CPDs. Our mapped lineaments also established a reliable fault/fracture network in the region as opposed to some of the inferred lineaments. Such intercalations of fault structures could positively aid geothermal exploration in the region

there are no prior temperature measurements at depths within the area of our CPD coverage. Therefore, we were challenged by the lack of data on the geothermal gradients and heat flow from deep wells to compare our estimated results. Nevertheless, we computed geothermal gradient and heat flow values using Eqs. 11 and 12 and compare results with data obtained from the Anambra Basin (located together with the Abakaliki Basin within the Lower Benue Trough; Onuoha and Ekine 1999). Estimated geothermal gradients realized using the CPD results gave values ranging from 29.0 to 45.0 °C km^{-1} with

an average of 36.3 $\pm$ 1.7 °C km^{-1} and heat flow estimates ranged between 52.2 to 101.5 mWm^{-2} with an average of 67.1 $\pm$ 2.3 mWm^{-2}. Our estimated geothermal gradient and heat flow values are within ranges of 25 to 49 $\pm$ 1 °C km^{-1} and 48 to 7 $\pm$ 63 mWm^{-2} (Onuoha and Ekine 1999) respectively obtained from deep wells drilled for oil exploration in the adjoining Anambra Basin. Heat flow values above 80 to 100 mWm^{-2} imply an anomalous geothermal situation in the subsurface (Sharma 2004; Abraham et al. 2014). Therefore, our estimated heat flow value
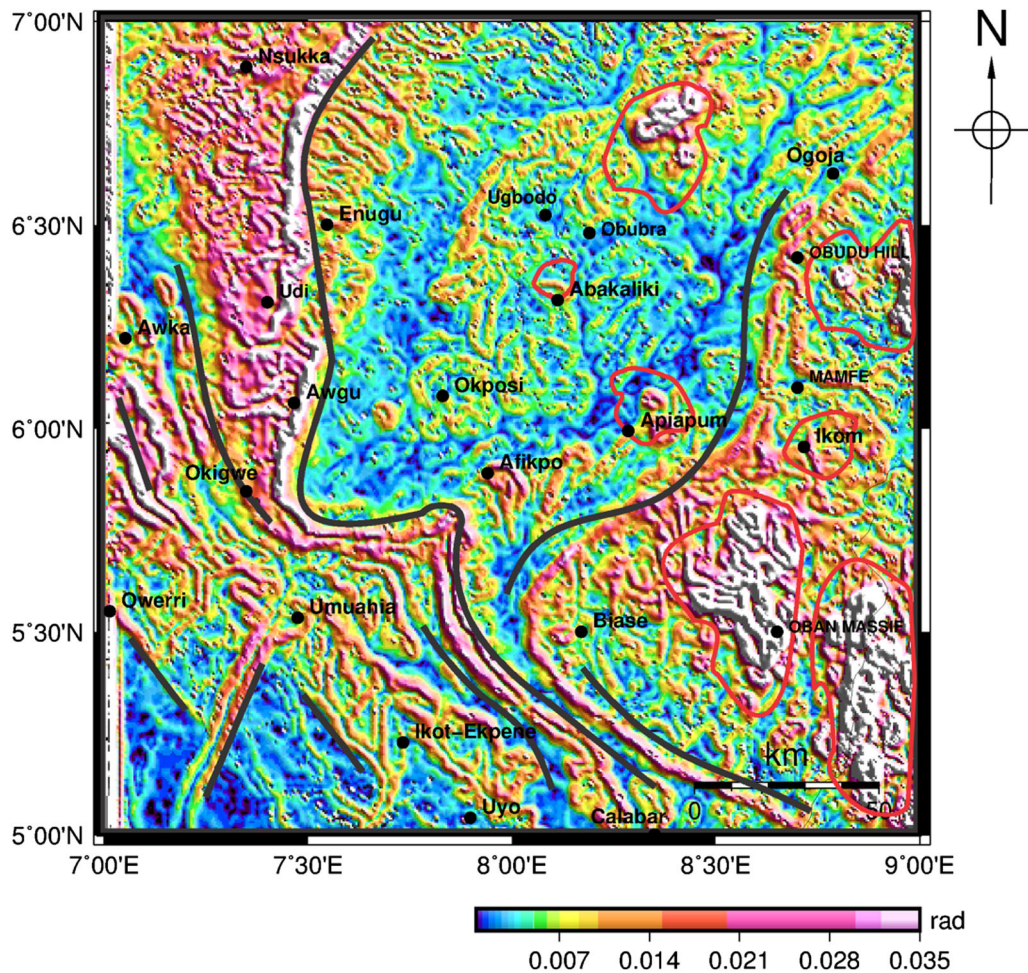
Figure 14
Improved normalized horizontal (INH) tilt angle map of the Bouguer anomalies. The locations of faults and geologic boundaries have been greatly enhanced by this map. The enclosed region (red line) identifies features which could represent subsurface intrusions; the black lines and curves identify faults/fractures and geologic boundaries/contacts, respectively

reiterates the viability of the region for further geothermal energy exploration.

Nigeria is not situated on any known seismic belt. However, between years 1993 and 2000, Nigeria experienced 15 seismic events, 3 of which occurred in one year. The intensities of these events range from III to IV based on the modified Mercalli Intensity Scale (Abraham et al. 2014). Of these events, only one event has been recorded in the region of this study, at Asaga-Ohafia near Umuahia, with local magnitudes between 3.7 and 4.2 and surface wave magnitudes of 3.7 to 3.9 (Ajakaiye et al. 1987; Eze et al. 2011). Our CPD estimates show decreasing depths along the Umuahia region and could also explain the epicenter location of earth tremors at that region. Once there are seismic activities, shallow CPDs could be observed unless there is an active rift in the region (Aboud et al. 2011).

Figure 9 shows a significant stretched feature of high-density positive gravity anomalies (amplitudes > 100 mGals) in the N–S and NW–SE directions in the region. This feature could be seen along Nsukka–Enugu–Udi–Awgu–Okigwe–Calabar regions and could be related to the high-density coal deposits in the region. Coal seams have been recorded for the Nsukka (Damian), Mamu (Maastrichtian)

and Asata Nkporo (Campano–Maastrichtian) Formations in the region (Obaje 1994). The Late Turonian–Early Santonian coal-bearing Awgu Formation lies conformably on the Eze Aku Formation. The Nkporo Formation, with its shale and poorly developed coals at the top, is transgressive and marine in origin, but passes upwards without any apparent break into the Mamu Formation (Obaje 2009). High-density positive anomalies (> 400 mGal) are also observed at the eastern and southeastern flanks of the map. These could be traced to the Precambrian basement complex at the Oban Massif and Obudu Hill regions. Gravity highs (within 20–250 mGal) spotted northwards of Obubra, and within Ugbodo–Abakaliki towns, are traced to the basic and intermediate intrusions within the Asu River Group. Significant gravity lows have also been noted around Obubra, Abakaliki, Afikpo, Apiapum, Ogoja and Mamfe regions. The gravity low aligning NE–SW from Afikpo to the Ogoja region is traced to the Turonian Eze-Aku Formation, younger than the adjoining westward Asu River Group (Albian–Cenomanian), with a majority concentration of positive (high-density) and low-density anomalies. We believe that the older Asu River Group formation was consolidated and compacted over time, resulting in reduced porosity and increased density as compared to the Eze-Aku Formation; hence the gravity highs.

Our estimated thickness of the crust (Moho; Fig. 10) varies from 26.5 to 35.8 km averaging at 29.6 km. Given the range of our CPD estimates, we propose that the thermal magnetic crust is located at the upper crust. We also note that the location with shallow depths to the Moho corresponded with the region of a lower CPD (Abakaliki region) and location with deeper Moho depths corresponded with that of a deeper CPD as observed around the Afikpo location. Shallow Moho depths have also been recorded in the southern region of the map around Calabar. To analyze subsurface tectonic interactions between all the estimated depths (depths to the top, centroid, CPD and Moho), results (Fig. 11) indicate that regions with shallow CPDs show some subsurface intrusions within. This can be seen clearly at Abakaliki (profile A) locations. We also observed decreasing depths to Moho (appearing as a slight rising) in profile A within locations of possible subsurface intrusions (Abakaliki). While on the contrary, the region around Afikpo (profile B), with deeper CPDs, shows increased depth to Moho (appearing as a depression) at the location. Since Moho depths were computed from the complete Bouguer gravity anomaly, independent of the magnetic data, the integrated outcome from this profile analysis could strengthen our depth estimations.

The TD maps (Fig. 12) reveal linear trends of acute density contrast throughout the region. We tender that some of these linear features are deep faults within the subsurface. This is another novel discovery brought about by our study as fault presence in the region was hitherto inferred. We traced some of these lineaments with inserted black lines on the map. The interpreted fault trends are mostly in the NE–SW and NW–SE directions. Our region of shallow CPD (Abakaliki) also had some notable faults traced. This study proposes a more reliable fault location and orientation in the region. The high-angle basin-bounding faults are only clearly evident in the gravity gradient response and this is significant for exploration of blind geothermal systems where faults do not have a surface expression in the cover geology (Kohrn et al. 2011). Lithological contacts have also been assumed for some of the linear features. A notable example is the lineation around the basement boundary at the Biase–Apiapum–Obudu Hill flank. The continuity of this lineation around Apiapum up to the Obudu Hill region (contrary to the superficial geological map) could signify deep lithological contact. A new lineament map (Fig. 13) has been developed for the region. Structures traced on the map were obtained from the TD map (black lines) of Fig. 12 and fault trends from the tectonic representation in Fig. 2 (red lines). From Fig. 13, we observed a concentration of faults around the region with deeper CPD (Awgu, Afikpo and Okposi towns) and also around the region of shallow CPD. The faults/fracture presence strengthens our proposal that the tectonic activity of the region could be responsible for the deeper and shallow CPDs obtained in the region. The heating effect of the volcanic and intrusive activity on Cretaceous sedimentary basins, especially the Benue Trough, as well as the basement complex contributed to the development of local thermal anomalies observed in the region (Kurowska

and Schoeneich 2010). The presence of these faults, especially within the region of shallow CPDs, could leverage geothermal exploration in the location. Faults could decide the success as well failure of low-enthalpy geothermal schemes. The ability of faults to function as pathways or baffles to geothermal fluid (or both simultaneosly) and their predominance throughout the subsurface explains the reasons for such properties (Loveless et al. 2014).

The prospective geothermal area could be deduced from total gradient analysis of gravity anomalies (Martakusumah et al. 2015). Figure 14 shows significant subsurface intrusions (marked in red) identified around Ugbodo, Obubra and Abakaliki locations. These locations have shallow CPDs due to subsurface intrusions in the Neocomian–Cenomanian Asu River Group of Albian age. On the eastern and southeastern flanks, we identified intrusions even within the undifferentiated basement complex with older granite presence. We propose the notable ridge structures around Umuahia, Owerri and Okigwe locations as pointers to the presence of normal faults in the region. We also propose that these intrusions could be responsible for the shallow CPDs in the region. Around the Afikpo region and extending downwards towards Umuahia, a lithological boundary/contact has been identified. This geologic feature is traced to one of the compressional folds that ensued in the mid-Santonian tectonic episode. This episode is believed to have affected the Benue Trough, resulting in the formation of anticlines and synclines (Benkhelil 1989). We interpret the mapped structures as one of the deformational structures identified as the Afikpo syncline in the study region. The elongated feature extending from Nsukka–Enugu–Udi–Awgu–Okigwe location is traced to the lower and upper coal measures of the Mamu and Nsukka Formations.

6. Conclusion

Analysis performed on aeromagnetic data over southeastern Nigeria has enabled us to identify locations with high geothermal prospects within the region. Spectral analysis technique applied on the data permits estimation of depths to the bottom of

magnetic sources herein assumed as CPDs. The study area is characterized by deeper CPDs (within an approximate range of 18.4–20.0 km) and shallow CPDs (within an approximate range of 9.7–17.4 km). Estimated geothermal gradients realized from computations using the CPD results gave values ranging from 29.0 to 45.0 $^{\circ}$C km^{-1} with an average of 36.3 $\pm$ 1.7 $^{\circ}$C km^{-1}. Heat flow estimates ranged between 52.2 and 101.5 mWm^{-2} with an average of 67.1 $\pm$ 2.3 mWm^{-2}. Our range of estimated geothermal gradients and heat flows agrees with the geothermal gradients and heat flow variations evaluated from deep wells drilled for oil exploration in the Anambra Basin (an adjoining sedimentary basin within the same geologic enclave). Shallow CPD regions (e.g. Abakaliki region) are associated with regions earlier identified to possess very high geothermal gradient trends in Nigeria. We propose that the shallow CPDs are due to basic and intermediate intrusions within the crust. This assertion has been corroborated by results from the gravity data analysis. The identified region with shallow CPDs is recommended for further geothermal exploration. Regions with shallow Moho depths (computed from gravity data) corresponded with that of shallow CPDs and deeper Moho, with deeper CPDs. Further analysis of the gravity data disclosed a subtle fracture network and interaction of the faults in the subsurface. As most of the faults and fractures in the region were inferred, our study has provided a dependable faults/fracture structure within the region. Faults/fractures identified at the shallow-CPD location could provide preferential pathways through the subsurface for circulation of geothermal fluid. We recommend further studies in the direction of examining drilled-hole temperatures and measured geothermal gradients along with possible application of seismic techniques to investigate further the various areas with high geothermal potential from our study.

R<small>EFERENCES</small>

Aboud, E., Salem, A., & Mekkawi, M. (2011). Curie depth map for Sinai Peninsula, Egypt deduced from the analysis of magnetic data. *Tectonophysics, 506,* 46–54.

Abraham, E. M., Lawal, K. M., Ekwe, A. C., Alile, O., Murana, K. A., & Lawal, A. A. (2014). Spectral analysis of aeromagnetic data for geothermal energy investigation of Ikogosi Warm Spring—Ekiti State, southwestern Nigeria. *Geothermal Energy, 2,* 1–21.

Abraham, E. M., & Nkitnam, E. E. (2017). Review of geothermal energy research in Nigeria: The geoscience front. *International Journal of Earth Science and Geophysics, 3,* 015.

Abraham, E. M., Obande, E. G., Mbazor, C., Chibuzo, G. C., & Mkpuma, R. O. (2015). Estimating depth to the bottom of magnetic sources at Wikki Warm Spring region, northeast Nigeria using fractal distribution of sources approach. *Turkish Journal of Earth Sciences, 24,* 1–19.

Abubakar, M. B. (2014). Petroleum Potentials of the Nigerian Benue Trough and Anambra Basin: A Regional Synthesis. *Natural Resources, 5,* 25–58.

Agagu, O. K., & Adighije, C. I. (1983). Tectonic and sedimentary framework of the lower Benue trough, Southeastern Nigeria. *Journal of African Earth Sciences, 1*(3/4), 267–274.

Ajakaiye, D. E. (1981). Geophysical investigation in the Benue-Trough. A review; Earth Evolution. Arbitrary shape; In: Computers in the Minerals industries. Part 1 (ed.) Parks G A, Stanford University Publ. Geol. Sci. 9: 464–480.

Ajakaiye, D. E., Daniyan, M. A., Ojo, S. B., & Onuoha, K. M. (1987). The southwestern Nigeria earthquake and its implications for the understanding of the tectonic structure of Nigeria. *Journal of Geodynamics, 7,* 205–214.

Ajibade, A. C., & Fitches, W. R. (1988). The Nigerian Precambrian and the Pan-African Orogeny. *Precambrian geology of Nigeria* (pp. 45–55). Abuja: A publication of the Nigerian Geological Survey Agency.

Avbovbo, A. A. (1978). Geothermal gradients in the Southern Nigerian Basin. *Bulletin of Canadian Petroleum Geology, 26*(2), 268–274.

Babalola, O. O. (1984). High-Potential geothermal energy resource areas of Nigeria and their geologic and geophysical assessment. *AAPG Bulletin, 68*(4), 450.

Bansal, A. R., Anand, S. P., Rajaram, M., Rao, V. K., & Dimri, V. P. (2013). Depth to the bottom of magnetic sources (DBMS) from aeromagnetic data of Central India using modified centroid method for fractal distribution of sources. *Tectonophysics, 603,* 155–161.

Bansal, A. R., Gabriel, G., Dimri, V. P., & Krawczyk, C. M. (2011). Estimation of depth to the bottom of magnetic sources by a modified centroid method for fractal distribution of sources: an application to aeromagnetic data in Germany. *Geophysics, 76,* L11–L22.

Baranov, V. (1957). A new method for interpretation of aeromagnetic maps: Pseudo-gravimetric anomalies. *Geophysics, 22,* 359–383.

Benkhelil, J. (1986). Caracteristiques structurales et evolution geodynamique du basin intracontinentale de la Benoue (Nigeria). Thesis d_etat, Nice, p. 275.

Benkhelil, J. (1989). The origin and evolution of the Cretaceous Benue Trough, Nigeria. *J Afr Earth Sci, 8,* 251–282.

Bhattacharyya, B. K., & Leu, L. K. (1975). Spectral analysis of gravity and magnetic anomalies due to two-dimensional structures. *Geophysics, 40,* 993–1013.

Bhattacharyya, B. K., & Morley, L. W. (1965). The delineation of deep crustal magnetic bodies from total field aeromagnetic anomalies. *Journal of Geomagnetism and Geoelectricity, 17,* 237–252.

Bilim, F. (2007). Investigations into the tectonic lineaments and thermal structure of Kutahya-Denizli region, western Anatolia, from using aeromagnetic, gravity and seismological data. *Physics of the Earth and Planetary Interiors, 165,* 135–146.

Blakely, R. J. (1988). Curie temperature analysis and tectonic implications of aeromagnetic data from Nevada. *Journal of Geophysical Research: Solid Earth, 93,* 11817–11832.

Blakely, R. J. (1995). *Potential theory in gravity and magnetic applications.* Cambridge: Cambridge University Press.

Chukwu, C. G., Udensi, E. E., Abraham, E. M., Ekwe, A. C., & Selemo, A. O. (2018). Geothermal energy potential from analysis of aeromagnetic data of part of the Niger-Delta Basin, Southern Nigeria. *Energy, 143,* 846–853. https://doi.org/10.1016/j.energy.2017.11.040.

Cordell, L. & Grauch, V. J. S. (1985). Mapping basement magnetization zones from aeromagnetic data in the San Juan Basin, New Mexico. In: Hinze, W. J. (Ed.), The utility of regional gravity and magnetic anomaly maps, Society of Exploration Geophysicists, 181–197.

Burke K., Dessauvagie, T. F. W. & Whiteman, A. J. (1972). Geological history of the Benue Valley and adjacent Areas. In Proceedings of the Conference on African Geology, 7–14 December, 1970, published by Department of Geology, University of Ibadan, Ibadan, Nigeria, pp. 187–205.

Dolmaz, M. N., Ustaomer, T., Hisarli, Z. M., & Orbay, N. (2005). Curie point depth variations to infer thermal structure of the crust at the African-Eurasian convergence zone, SW Turkey. *Earth Planets Space, 57,* 373–383.

Emujakporue, G. O., & Nwosu, L. I. (2017). Subsurface temperature prediction from multilayer solution of heat flow equation: a case study of Anambra Sedimentary Basin, Nigeria. *IOSR Journal of Applied Geology Geophysics, 5*(2), 60–67.

Eppelbaum, L., & Katz, Y. (2015a). Eastern Mediterranean: Combined geologicalegeophysical zonation and paleogeodynamics of the Mesozoic and Cenozoic structural-sedimentation stages. *Marine and Petroleum Geology, 65,* 1–19.

Eppelbaum, L., & Katz, Y. (2015b). Newly developed paleomagnetic map of the Easternmost Mediterranean joined with tectonostructural analysis unmask geodynamic history of this region. *Open Geosci., 7,* 95–117.

Eppelbaum, L. & Katz, Y. (2017). Satellite gravity transforms unmask tectonic pattern of Arabian—African region. Geophysical Res. Abstracts, 19: EGU2017-2908-1.

Eze, C. L., Sunday, V. N., Ugwu, S. A, Uko, E. D. & Ngah, S. A. (2011). Mechanical model for Nigerian intraplate earth tremors., Earthzine. http://www.earthzine.org/2011/05/17/mechanical-model-for-nigerian-intraplate-earth-tremors.

Georgsson, L. S. (2009). Geophysical methods used in geothermal exploration. Presented at Short Course IV on Exploration for Geothermal Resources, organized by UNU-GTP, KenGen and GDC, at Lake Naivasha, Kenya, November 1–22.

Gottsmann, J., Camacho, A. G., Martí, J., Wooller, L., Fernández, J., García, A., et al. (2008). Shallow structure beneath the Central Volcanic Complex of Tenerife from new gravity data:

implications for its evolution and recent reactivation. *Physics of the Earth and Planetary Interiors, 168,* 212–230.

Hoque, M., & Nwajide, C. S. (1985). Tectono-sedimentological evolution of an elongate intracratonic basin (aulacogen): The case of the Benue Trough of Nigeria. *Journal of Mining and Geology, 21,* 19–26.

Jain, S. (1988). Total magnetic field reduction—The Pole or Equator? A model study. *Canadian Journal of Exploration Geophysics, 24*(2), 185–192.

Kogbe, C. A., & Obialo, A. U. (1976). Statistics of mineral production in Nigeria (1946–1974) and the contribution of the mineral industry to the Nigerian economy. In C. A. Kogbe (Ed.), *Geology of Nigeria* (pp. 391–428). Lagos: Elizabethan Publishers.

Kohrn, B., Bonet, C., DiFrancesco, D., & Gibson, H. (2011). Geothermal exploration using gravity gradiometry—A Salton Sea example. Geothermal Resources Council Transactions Volume 35. GRC Annual Meeting (2011).

Kurowska, E.& Schoeneich, K. (2010). Geothermal exploration in Nigeria, Proceedings of World Geothermal Congress, Bali, Indonesia, 25–29.

Leu, L. K. (1981). Use of reduction-to-the-equator process for magnetic data interpretation: Presented at the 51st Ann. Int. Mtg., Soc. Expl. Geophy., Los Angeles, Abstract P. 12, Geophysics 47, 445.

Li, L., Huang, D., Han, L., & Ma, G. (2014). Optimised edge detection filters in the interpretation of potential field data. *Exploration Geophysics, 45,* 171–176.

Loveless, S., Pluymaekers, M., Lagrou, D., De Boever, E., Doomenbal, H., & Laenen, B. (2014). Mapping geothermal potential of fault zones in the Belgium-Netherlands Border region. *Energy Procedia, 59,* 351–358.

Maden, N. (2009). Crustal thermal properties of the Central Pontides (Northern Turkey) deduced from spectral analysis of magnetic data. *Turkish Journal of Earth Sciences, 18,* 1–10.

Manea, M., & Manea, V. C. (2011). Curie point depth estimates and correlation with subduction in Mexico. *Pure and Applied Geophysics, 168,* 1489. https://doi.org/10.1007/s00024-010-0238-2.

Manzella, A. (2009). Geophysical methods in geothermal exploration. Italian National Research Council. http://hendragrandis.files.wordpress.com/2009/04/a_manzella.pdf.

Martakusumah, R., Suryantini, W. S., Pratama, A. B. & Haans, A. (2015). Gravity analysis for hidden geothermal system in Cipanas, Tasikmalaya Regency, West Java. Proceedings World Geothermal Congress 2015, Melbourne, Australia, 19–25.

Mayhew, M. A. (1985). Curie isotherm surfaces inferred from high altitude magnetic anomaly data. *Journal of Geophysical Research: Solid Earth, 90*(B3), 2647–2654.

Miller, H. G., & Singh, V. J. (1994). Potential Field tilt—A new concept for location of potential field sources. *Applied Geophysics, 32,* 213–217.

Mishra, D. C., Kuma, M. R., & Arora, K. (2012). Long wavelength satellite gravity and geoid anomalies over Himalaya and Tibet: Lithospheric structures and seismotectonics of deep focus earthquakes of Hindu Kush—Pamir and Burmese arc. *Journal of Asian Earth Sciences, 48,* 93–110.

Mohammadzadeh-Moghaddam, M., Mirzaei, S., Nouraliee, J., & Porkhial, S. (2016). Integrated magnetic and gravity surveys for geothermal exploration in Central Iran. *Arabian Journal of Geosciences, 9,* 506.

Montesinos, F. G., Camacho, A. G., Nunes, J. C., Oliveira, C. S., & Vieira, R. (2003). A 3-D gravity model for a volcanic crater in Terceira Island (Azores). *Geophysical Journal International, 154,* 393–406.

Murat, R. C. (1972). Stratigraphy and paleogeography of the Cretaceous and Lower Tertiary in southern Nigeria. In T. F. J. Dessauvagie & A. J. Whiteman (Eds.), *African Geology* (pp. 251–266). Nigeria: University of Ibadan Press.

Nishijimaa, J., & Naritomi, K. (2017). Interpretation of gravity data to delineate underground structure in the Beppu geothermal field, central Kyushu, Japan. *Journal of Hydrology: Regional Studies, 11,* 84–95.

Nur, A. (2000). Analysis of aeromagnetic data over the Yola arm of the Upper Benue Trough, Nigeria. *Journal of Mining and Geology, 36,* 77–84.

Nur, A., Ofoegbu, C. O., & Onuoha, K. M. (1999). Estimation of the depth to the Curie point Isotherm in the upper Benue Trough, Nigeria. *Journal of Mining and Geology, 35*(1), 53–60.

Nwachukwu, S. O. O. (1975). Geothermal regime of southern Nigeria. GRC Geothermal Library. pubs.geothermal-library.org/lib/grc/1005046.pdf (Proceedings: Secon UN symposium on the development and use of geothermal resources, 1: 205–212.

Nwachukwu, S. O. (1976). Approximate geothermal gradients in Niger Delta Sedimentary Basin. *AAPG Bulletin, 60*(7), 1073–1077.

Obaje, N. G. (1994). Coal petrography, microfossils and paleoenvironments of Cretaceous coal measures in the Middle Benue Trough of Nigeria. *Tuebinger Mikropalaeontologische Mitteilungen, 11,* 1–165.

Obaje, N. G. (2009). Geology and mineral resources of Nigeria. Lecture notes in earth sciences. S. Bhattacharji, Brooklyn, H. J. Neugebauer, Bonn, J. Reitner, Göttingen, K. Süwe, Graz.

Obande, G. E., Lawal, K. M., & Ahmed, L. A. (2014). Spectral analysis of aeromagnetic data for geothermal investigation of Wikki Warm Spring, north-east Nigeria. *Geothermics, 50,* 85–90.

Obi, D. A., Okereke, C. S., Obei, B. C., & George, A. M. (2010). Aeromagnetic modelling of subsurface intrusives and its implication on hydrocarbon evaluation of the Lower Benue Trough, Nigeria. *European Journal of Science and Research, 47,* 347–361.

Obi, G. C., Okogbue, C. O., & Nwajide, C. S. (2001). Evolution of the Enugu Cuesta: A tectonically driven erosional process. *Global Journal of Pure Applied Sciences, 7,* 321–330.

Obiora, S. C., & Charan, S. N. (2010). Tectonomagmatic origin of some volcanic and sub-volcanic rocks from the Lower Benue rift. *Nigeria. Journal African Earth Sciences., 58,* 197–210.

Oboh-Ikuenobe, F. E., Obi, C. G., & Jaramillo, C. A. (2005). Lithofacies, palynofacies, and sequence stratigraphy of Palaeogene strata in Southeastern Nigeria. *Journal of African Earth Sciences, 41,* 79–101.

Ofoegbu, C. O. (1984). Interpretation of aeromagnetic anomalies over the Lower and Middle Benue Trough of Nigeria. *Geophysical Journal of the Royal Astronomical Society, 79,* 813–823.

Ofoegbu, C. O. (1985). A review of the geology of the Benue Trough of Nigeria. *Journal of African Earth Sciences, 3,* 283–291.

Ofoegbu, C. O., & Onuoha, K. M. (1991). Analysis of magnetic data over the Abakaliki Anticlinorium of the lower Benue Trough, Nigeria. *Marine and Petroleum Geology, 8*(2), 174–183.

Oha, I. A., Onuoha, K. M., Nwegbu, A. N., & Abba, A. U. (2016). Interpretation of high-resolution aeromagnetic data over southern Benue Trough, southeastern Nigeria. *Journal of Earth System Science, 125*(2), 369–385.

Okubo, Y., Graf, R. J., Hansen, R. O., Ogawa, K., & Tsu, H. (1985). Curie point depths of the Island of Kyushu and surrounding areas, Japan. *Geophysics, 53*(3), 481–494.

Okubo, Y., & Matsunaga, T. (1994). Curie point depth in northeast Japan and its correlation with regional thermal structure and seismicity. *Journal of Geophysical Research: Solid Earth, 99,* 22363–22371.

Okubo, Y., Matsushima, J., & Correia, A. (2003). Magnetic spectral analysis in Portugal and its adjacent seas. *Physics and Chemistry of the Earth, 28,* 511–519.

Onuoha, K. M., & Ekine, A. S. (1999). Subsurface temperature variation and heat flow in the Anambra Basin, Nigeria. *Journal of African Earth Sciences, 28*(3), 641–652.

Osazuwa, I. B., Ajakaiye, D. E., & Verheijen, P. J. T. (1981). Analysis of the structure of part of the Upper Benue Rift Valley on the basis of new geophysical data. *Tectonophysics, 2,* 126–134.

Petters, S. W. (1982). Central West African Cretaceous-Tertiary benthic foraminifera and stratigraphy. *Palaeontographica Abt, 179,* 1–104.

Rajaram, M., Anand, S. P., Hemant, K., & Purucker, M. E. (2009). Curie isotherm map of Indian subcontinent from satellite and aeromagnetic data. *Earth and Planetary Science Letters, 281,* 147–158.

Represas, P., Santos, F. A., & Ribeiro, J. (2013). Interpretation of gravity data to delineate structural features connected to low-temperature geothermal resources at Northeastern Portugal. *Journal of Applied Geophysics, 92,* 30–38.

Riad, S., Refai, E., & Ghalib, M. (1981). Bouguer anomalies and crustal structure in the Eastern Mediterranean. *Tectonophysics, 71,* 253–266.

Rivas, J. (2009). Gravity and magnetic methods, short course on surface exploration for geothermal resources. UNU-GTP and LaGeo, in Ahuachapan and Santa Tecla. 1–13.

Ross, H. E., Blakely, R. J., & Zoback, M. D. (2006). Testing the use of aeromagnetic data for the determination of Curie depth in California. *Geophysics, 71*(5), L51–L59.

Salem, A., Furuya, S., Aboud, E., Elawadi, E., Jotaki, H. & Ushijima, K. (2005). Subsurface structural mapping using gravity data of Hohi Geothermal Area, Central Kyushu, Japan. Proceedings World Geothermal Congress, Antalya, Turkey.

Salem, A., Ushijima, K., Elsiraft, A.& Mizunaga, H. (2000). Spectral, analysis of aeromagnetic data for geothermal reconnaissance of,Quseir area, northern Red Sea, Egypt. Proceedings of the world geothermal congress: 1669–1674.

Sandwell, D. T., Garcia, E., Soofi, K., Wessel, P., & Smith, W. H. F. (2013). Towards 1 mGal Global marine gravity from CryoSat-2, Envisat, and Jason-1. *The Leading Edge, 32*(8), 892–899. https://doi.org/10.1190/tle32080892.1.

Sandwell, D. T., Muller, R. D., Smith, W. H. F., Garcia, E., & Francis, R. (2014). New global marine gravity model from CryoSat-2 and Jason-1 reveals buried tectonic structure. *Science, 346*(6205), 65–67.

Sandwell, D. T., & Smith, W. H. F. (2009). Global marine gravity from retracked Geosat and ERS-1 altimetry: Ridge segmentation versus spreading rate. *Journal of Geophysical Research: Solid Earth, 114,* B01411. https://doi.org/10.1029/2008jb006008.

Sharma, P. V. (2004). *Environmental and engineering geophysics* (p. 475). Cambridge: Cambridge University Press.

Short, K. C., & Stauble, A. J. (1967). Outline of geology of Niger delta. *American Association of Petroleum Geologists Bulletin, 51,* 761–779.

Shuey, R. T., Schellinger, D. K., Tripp, A. C., & Alley, L. B. (1977). Curie depth determination from aeromagnetic spectra. *Geophysical Journal International, 50,* 75–101.

Soengkono, S. (2011). Deep interpretation of gravity and airborne magnetic Data over the Central Taupo Volcanic Zone, New Zealand Geothermal Workshop.

Spector, A., & Grant, F. S. (1970). Statistical models for interpreting aeromagnetic data. *Geophysics, 35,* 293–302.

Stampolidis, A., & Tsokas, G. (2002). Curie point depths of Macedonia and Thrace, N. Greece. *Pure and Applied Geophysics, 159,* 1–13.

Tanaka, A., Okubo, Y., & Matsubayashi, O. (1999). Curie-temperature isotherm depth based on spectrum analysis of the magnetic anomaly data in east and southwestern Asia. *Tectonophysics, 306,* 461–470.

Thurston, J. B., & Smith, R. S. (1997). Automatic conversion of magnetic data to depth, dip and susceptibility contrast using the SPITM method. *Geophysics, 62,* 807–813.

Trifonova, P., Zheler, Z., & Petrova, T. (2006). Curie point depths of the Bulgarian territory inferred from geomagnetic observations. *Bulgarian Geophysical Journal, 32,* 12–23.

Trifonova, P., Zheler, Z., Petrova, T., & Bojadgieva, K. (2009). Curie point depths of the Bulgarian territory inferred from geomagnetic observations and its correlation with regional thermal structure and seismicity. *Tectonophysics, 473,* 362–374.

Tsokas, G., Hansen, R. O., & Fyticas, M. (1998). Curie point depth of the Island of Crete (Greece). *Pure and Applied Geophysics, 159,* 1–13.

Verduzco, B., Fairhead, J. D., Green, C. M., & MacKenzie, C. (2004). New insights into magnetic derivatives for structural mapping. *The Leading Edge, 23,* 116–119.